

SUPPLEMENT TO THE GEOLOGIC MAP OF THE CARNATION 7.5-MINUTE QUADRANGLE, KING COUNTY, WASHINGTON— GEOCHRONOLOGIC, GEOCHEMICAL, POINT COUNT, GEOPHYSICAL, EARTHQUAKE, FAULT, AND NEOTECTONIC DATA

by Joe D. Dragovich,
Megan L. Anderson,
James H. MacDonald, Jr.,
Shannon A. Mahan,
S. Andrew DuFrane,
Heather A. Littke,
Gregory R. Wessel,
Jennifer H. Saltonstall,
Curtis J. Koger,
and Recep Cakir

WASHINGTON
DIVISION OF GEOLOGY
AND EARTH RESOURCES
Open File Report 2010-2
June 2010

*This report has not been edited or reviewed for
conformity with Division of Geology and Earth Resources
standards or geologic nomenclature*



WASHINGTON STATE DEPARTMENT OF
Natural Resources

Peter Goldmark - Commissioner of Public Lands

DISCLAIMER

Neither the State of Washington, nor any agency thereof, nor any of their employees, makes any warranty, express or implied, or assumes any legal liability or responsibility for the accuracy, completeness, or usefulness of any information, apparatus, product, or process disclosed, or represents that its use would not infringe privately owned rights. Reference herein to any specific commercial product, process, or service by trade name, trademark, manufacturer, or otherwise, does not necessarily constitute or imply its endorsement, recommendation, or favoring by the State of Washington or any agency thereof. The views and opinions of authors expressed herein do not necessarily state or reflect those of the State of Washington or any agency thereof.

**WASHINGTON STATE DEPARTMENT OF
NATURAL RESOURCES**

Peter Goldmark—*Commissioner of Public Lands*

DIVISION OF GEOLOGY AND EARTH RESOURCES

David K. Norman—*State Geologist*

John P. Bromley—*Assistant State Geologist*

Washington Department of Natural Resources
Division of Geology and Earth Resources

Mailing Address:

MS 47007
Olympia, WA 98504-7007

Street Address:

Natural Resources Bldg, Rm 148
1111 Washington St SE
Olympia, WA 98501

Phone: 360-902-1450

Fax: 360-902-1785

E-mail: geology@dnr.wa.gov

Website: <http://www.dnr.wa.gov/AboutDNR/Divisions/GER/>

This and other DGER publications are available online at:

[http://www.dnr.wa.gov/ResearchScience/Topics/GeologyPublicationsLibrary/
Pages/pubs.aspx](http://www.dnr.wa.gov/ResearchScience/Topics/GeologyPublicationsLibrary/Pages/pubs.aspx)

The online catalog and bibliography of the Washington Geology Library is at:

[http://www.dnr.wa.gov/ResearchScience/Topics/GeologyPublicationsLibrary/
Pages/washbib.aspx](http://www.dnr.wa.gov/ResearchScience/Topics/GeologyPublicationsLibrary/Pages/washbib.aspx)

Suggested Citation: Dragovich, J. D.; Anderson, M. L.; MacDonald, J. H., Jr.; Mahan, S. A.; DuFrane, S. A.; Littke, H. A.; Wessel, G. R.; Saltonstall, J. H.; Koger, C. J.; Cakir, Recep, 2010, Supplement to the geologic map of the Carnation 7.5-minute quadrangle, King County, Washington—Geochronologic, geochemical, point count, geophysical, earthquake, fault, and neotectonic data: Washington Division of Geology and Earth Resources Open File Report 2010-2, 42 p., 8 digital appendices.

Published in the United States of America

© 2010 Washington Division of Geology and Earth Resources

Supplement to the Geologic Map of the Carnation 7.5-minute Quadrangle, King County, Washington—Geochronologic, Geochemical, Point Count, Geophysical, Earthquake, Fault, and Neotectonic Data

by Joe D. Dragovich¹, Megan L. Anderson², James H. MacDonald Jr.³, Shannon A. Mahan⁴, S. Andrew DuFrane⁵,
Heather A. Littke¹, Gregory R. Wessel⁶, Jennifer H. Saltonstall⁷, Curtis J. Koger⁷, and Recep Cakir¹

Geochemical Laboratory Analysts:

Diane J. Cornelius⁸, Richard M. Conrey⁸, and Charles M. Knaack⁸

Tephrochronologist:

Franklin F. (Nick) Foit, Jr.⁹

JUNE 2010

1 Washington Division of Geology and Earth Resources
MS 47007
Olympia, WA 98504-7007

2 Colorado College
Department of Geology
14 E Cache La Poudre St
Colorado Springs, CO 80903

3 Florida Gulf Coast University
Department of Marine and Ecological Science
Fort Myers, FL 33965

4 U.S. Geological Survey
Box 25046 MS 974
Denver Federal Center
Denver, CO 80225-5046

5 University of Alberta
Department of Earth and Atmospheric Sciences
1-26 Earth Sciences Building
Edmonton Canada T6G 2E3

6 King County Department of Development and
Environmental Services
900 Oakesdale Ave SW
Renton, WA 98057

7 Associated Earth Sciences, Inc.
911 5th Avenue, Suite 100
Kirkland, WA 98033

8 Washington State University School of Earth
and Environmental Sciences
GeoAnalytical Laboratory
PO Box 642812
Pullman, WA 99164-2812

9 Electron Beam Facility
Washington State University School of
Earth and Environmental Sciences
GeoAnalytical Laboratory
PO Box 642812
Pullman, WA 99164-2812

INTRODUCTION

The reader is urged to examine the following data and analyses in conjunction with the geologic map of the Carnation 7.5-minute quadrangle by Dragovich and others (2010). The Carnation quadrangle document provides the geologic overview, geologic rock unit list and unit symbology as well as the locations of some of the sites mentioned herein including the locations of the sand point count samples, IRSL age sites, some of the radiocarbon age sites, and some of the neotectonic sites. Geologic mapping of the Carnation quadrangle is part of our broader effort to provide detailed geologic map information in the Snoqualmie Valley area (Dragovich, 2007; Dragovich and Walsh, 2008; Dragovich and others, 2007, 2009a,b,c, 2010). Several electronic appendices and figures accompany this report as outlined in Table 1.

Table 1. Location and brief description of appendices, tables, or figures cited in this report.

Table, appendix, or figure no.	File name (attachments)	Notes
Appendix 1	a1_radiocarbon_data_carnation.docx	Radiocarbon ages in and near the Carnation 7.5-minute quadrangle (this study and previous Associated Earth Sciences, Inc. studies)
Appendix 2	a2_geochemical_data_carnation.xls	Geochemical data, petrography and sample information; note appendix contains three tabs with the third tab presenting basic sample information including petrography notes; also see Appendices 3-4
Appendix 3	a3_geochemical_sample_locations_carnation.pdf	Geochemical sample site locations in the Carnation 7.5-minute quadrangle; also see location descriptions and other sample notes provided in Appendix 2
Appendix 4	a4_geochemical_data_plots_carnation.pdf	Seven additional geochemical plots; also see Figures 1A-1D
Appendix 5	a5_bedrock_top_contour_map_carnation.pdf	Bedrock top contour map of the Carnation 7.5-minute quadrangle
Appendix 6	a6_u_pb_geochronology_carnation.xls	Single zircon U-Pb data, plots and sample information; note spreadsheet contains multiple tabs
Appendix 7	a7_neotectonic_photos_carnation.pdf	Outcrop photos of deformational and liquefaction features in Quaternary deposits
Appendix 8	a8_major_fault_attributes_carnation.xls	Fault attributes including certainty, activity, previous mapping and other characteristics for faults mapped by Dragovich and others (2010)
Figure 1A-1D	Embedded in this document	Geochemical plots; see Appendix 4 for additional plots
Figure 2A-2D	Embedded in this document	Isostatic gravity and aeromagnetic map of the Carnation quadrangle and geophysical Cross Sections A and B; see Cross Sections A and B of Dragovich and others (2010) for our stratigraphic interpretation of the cross sections
Figures 3A-3D	Embedded in this document	Hypocenter maps of the Carnation quadrangle and part of the Lake Joy 7.5-minute quadrangle and hypocenter Cross Sections A and B; see Plate 1 of Dragovich and others (2010) for geologic mapping of the area
Figure 4	Embedded in this document	Cartoon showing basin inversion model for the Olympia Beds in the Snoqualmie Valley
Table 2	Embedded in this document	IRSL age data table for the Olympia bed and Whidbey Formation samples in the Carnation 7.5-minute quadrangle
Table 3	Embedded in this document	Composition and correlation information for a Whidbey Formation tephra in the Carnation 7.5-minute quadrangle
Table 4	Embedded in this document	Major Quaternary provenances for glacial and nonglacial deposits in the Carnation quadrangle area

RADIOCARBON GEOCHRONOLOGY

Details about the radiocarbon ages cited in Dragovich and others (2010) are provided in Appendix 1. The table also provides additional radiocarbon age information sampled from units Qa (alluvium), Qc_{ol} (Olympia beds), and Qc_{pr} (Pre-Fraser nonglacial) by Associated Earth Sciences, Inc. (AESI) west of the Carnation quadrangle. These samples were obtained in the adjacent Redmond 7.5-minute quadrangle on Redmond Ridge and in the Snoqualmie Valley. Several of these radiocarbon age sites are within a few hundred to a few thousand feet of the Carnation quadrangle. These ages, combined with stratigraphic and compositional information, demonstrate that unit Qc_{ol} on southeast Union Hill and eastern-most Redmond Ridge is a relatively thin nonglacial unit (~0-50 ft thick) that correlates with the Olympia nonglacial interval. Examination of sands from AESI borings indicates that the sediments are locally derived fluvial deposits. Olympia-age deposits thicken to over 80 feet beneath much of Redmond Ridge approximately 1 mile west of the Carnation Quadrangle.

“Infinite” radiocarbon ages cited in Appendix 1 are derived from organic materials that are older than the limit of the radiocarbon dating method (greater than ~44,000 yrs B.P. or ~44 ka). Our assignment of the strata with “infinite” ages to the Olympia nonglacial interval (Olympia beds) south of Duvall (age sites 41C and 41E) was made on the basis of Snoqualmie River provenance sand composition (Table 4) and inferred stratigraphic position above Possession glacial drift. The correlation of the underlying glacial drift with the Possession glaciation is made on the basis of weathering characteristics (for example, rind thickness). However, such a correlation is tenuous and this moderately weathered sediment could be Double Bluff glacial drift (unit Qgd_d), which would result in a correlation of the SP sediments with deposits of the next oldest nonglacial interval, which is the Whidbey Formation. Infinite ages obtained from pre-Fraser ancient Snoqualmie River provenance sediments (unit Qc_{pr}) could be Olympia beds, Whidbey Formation, or an older nonglacial Snoqualmie provenance unit. Our new Single Infrared Stimulated Luminescence age date of 48 ka (described below) shows that at least some of the Snoqualmie provenance sediments older than the radiocarbon age dating limit of ~44 ka are Olympia beds.

SINGLE INFRARED STIMULATED LUMINESCENCE AGES FOR THE OLYMPIA BEDS AND WHIDBEY FORMATION

Methodology

GENERAL CONCEPTS OF LUMINESCENCE DATING

Most minerals react to ionizing radiation by essentially gaining energy at the electron level, which accumulates through time if that energy is not released (as light) by some outside stimuli (sunlight or intense heat over 200°C). Thus, sediment grains can record their exposure history to ionizing radiation, which can then be “read” in the laboratory and used as a clock. This procedure is referred to as luminescence geochronology, the goal of which is to establish the timing of the burial of mineral grains in sedimentary deposits. Luminescence dating is based on solid-state dosimetric properties of natural mineral grains. Minerals react to ionizing radiation, which is generated by radioactive isotopes found in minor quantities in most terrestrial sediments and by cosmic radiation. Specifically, ionizing radiation creates charge pairs/carriers (e⁻, h⁺) in mineral crystals. The charge carriers are mobile within the crystals, but can become localized, or trapped, at lattice defects and held there over geologically significant time scales. Over time, the number of segregated, or trapped, charge carriers builds up in a way that can be described by a saturating exponential function. If the mineral grains were transported at night, in turbid fluvial conditions, or were generally considered to be deposited in massive, sudden discharge events (i.e. debris flows, colluvium, etc.) luminescence dating may produce depositional ages that are too old because the luminescence clock was not reset to “zero” prior to burial. Exposure to heat, light, or high pressures can release charge carriers from trapping sites and permit recombination, during which light is emitted from the mineral grains. This detrapping resets the system within the mineral grains. In terrestrial environments exposure to sunlight during sediment transport resets the clock and it is also why a luminescence age is considered a burial age. In the laboratory, sediment is stimulated to emit light, which is measured. The sediment is stimulated by exposure to light of specific wavelengths (optically stimulated luminescence,

OSL), or heat (thermoluminescence, TL), in proscribed manners. The intensity of emitted light measured in the laboratory is proportional to the trapped charge population, which is proportional to the total absorbed radiation dose (D_e) that the sedimentary deposit experienced, and that relation is proportional to the time elapsed since burial. The simplest form of the OSL age equation is:

$$t_{OSL} = \frac{D_e}{D'}$$

where

t_{OSL} = age

D_e = total absorbed radiation dose,

D' = natural environmental dose rate.

A dose rate model was constructed that assumed moisture contents of about 60% of full saturation (i.e. 26% of a possible 44%). This simple model should account for seasonal moisture variations, water content, and dose rate analysis as described by Mahan and others (2007) using methods modified from Aitken (1985), Murray and others (1987), and Snyder and Duval (2003).

SAMPLE COLLECTION

IRSL samples were collected from freshly cleaned natural exposures for luminescence processing. At least 50 cm of sediment was removed from the face of each exposure before sampling to minimize the possibility of bleaching of the outer layers of the sediment by sunlight. Opaque plastic tubes ~ 20 cm-long, were hammered perpendicular into the exposed vertical faces to extract the sediment samples. The tubes were sealed and placed in light-proof photographic bags until the initial processing. All samples were processed at the USGS luminescence laboratory in Denver, Colorado

DETERMINING THE EQUIVALENT DOSE (D_e)

At least 5 cm of sediment was removed from both ends of the sampling tube under “safe light” (sodium vapor lighting) conditions in the luminescence laboratory. The ends and the middle portion of the samples were dried in an oven at 30°C. The entire sample was leached in 4M HCl (10% HCl) for 24 hours, 30% H_2O_2 for 24 hours, and 10% HF for 20 minutes. There were no coarser sized grains (<170 mesh or 90 microns) and thus the finer silt-size grains were used for IRSL dating. This type of luminescence stimulates only the feldspars even if those grains are in a polymineral mix.

IRSL was done on a polymineralic fine silt fraction (4-11 μm). The silt was preheated using a long, slow temperature of 124°C for 64 hours. IRSL analyses were performed on a Daybreak 1100 luminescence reader with Schott BG-39 filters coupled to an EMI 9635 QA Photomultiplier tube. The silt was dated using the total-bleach multiple-aliquot additive-dose (MAAD) method (Singhvi and others, 1982; Richardson and others, 1997; Forman and Pierson, 2002). A minimum of two analyses per IRSL sample by MAAD methods was performed. Anomalous fading tests on the stability of the luminescence signal indicated little to no signal instability (recording ratios of 0.91 to 1.00 for a fade ratio of only 1 to 2 percent). Growth curve data were fit to an exponential trend. All samples were analyzed using continuous wave (CW-OSL) stimulation. The sample size for the silt-sized particles was on the order of many thousands of grains (but no actual count was attempted), covering the entire disc surface.

DETERMINING THE DOSE RATE (D_R)

Most ionizing radiation in the sediment is from the decay of isotopes in the uranium and thorium decay chains and the radioactive potassium-40 element. The dose rate was obtained by elemental data analyses. The concentrations of K, U, Th, and Rb were determined using gamma spectrometry following the procedures described in Snyder and Duvall (2003). The bulk samples were dried, homogenized by gentle disaggregation, weighed, sealed in plastic planchets having a diameter of 15.2 cm by 3.8 cm (some

modification from Murray and others, 1987), and then immediately placed in a low-resolution NaI detector gamma-ray spectrometer at the USGS Gamma Spectrometry Lab in Denver for about 8.5 hours. Samples were then stored for a minimum of twenty-one days to allow radon to achieve radioactive equilibrium, and the measurements were repeated. The fraction of radon emanation was estimated from the difference of these two spectrometer measurements. A sealed/unsealed ratio of <1.10 is not considered to represent significant radon escape under laboratory conditions. These count rates are accurate for calculating dose rates. Alpha and beta contributions to the dose rate were corrected for grain-size attenuation (Aitken, 1985). The alpha efficiency for the silt-sized samples was determined by comparing MAAD-alpha source exposed and MAAD-beta source exposed curves, using approaches in Aitken (1985). Measured elemental concentrations, associated dose rates, and cosmic ray contributions are presented in Table 2. Cosmic-ray dose rate data was estimated for each sample as a function of depth, elevation above sea level, and geomagnetic latitude (Prescott and Hutton, 1994).

Sample Site Descriptions and Results

IRSL ages for samples 09-81Z and WA-47 are presented in Table 2. These ages suggest that these samples are correlative with the Olympia beds and the Whidbey Formation, respectively.

OLYMPIA BEDS

Sample 81Z is located in Cherry Valley, a few miles east of Duvall, Washington (N 47°44.669', W 121°57.138'; age site 81Z of Dragovich and others, 2010). The sample was obtained from a steep road cut along Cherry Valley Road about 1-1.5 meters below the soil horizon. The road cut exposes orange brown, thinly to thickly bedded medium sand to silty sand to silt with thin beds of brown clay locally. Some disseminated organics occur locally in these fluvial overbank deposits. Petrographic examination of this sand indicates that this alluvium is rich in monocrystalline quartz grains with significant potassium feldspar grains, plagioclase and lesser polycrystalline quartz and lithic grains. Sediment provenance is ancient Snoqualmie River alluvium and contains accessory hornblende and biotite typical of ancient Snoqualmie River alluvium (unit Qc_o in Table 4). Deposits are fractured, tilted and open-folded probably as a result of tectonic deformation near the Cherry Valley fault. The deposits are also intensely liquefied and display flame structures and convolute bedding. The IRSL age was obtained from the detrital potassium feldspar grains (fine silt fraction). The IRSL age of 48 ka (48,000 yrs B.P.) indicates that this nonglacial sediment correlates with the Olympia beds (Table 2).

WHIDBEY FORMATION

Sample WA-47 is located on Union Hill at an elevation of ~255 ft in the Carnation 7.5-minute quadrangle—NW corner of T25N R6E, Section 1 along an abandoned logging road at age site WA-47 of Dragovich and others (2010). The road cut exposes well-stratified and thinly bedded fine to coarse micaceous sand and silt with minor beds of laminated clay of the Whidbey Formation (unit Qc_{ws}). The sample is petrographically and geochemically similar to other ancient Snoqualmie River alluvium samples that we have obtained both locally and regionally (Table 4). Sample WA-47 was originally sampled by Associated Earth Sciences for thermoluminescence (TL) dating in 2005 (Koger and Saltonstall, 2009). See geochemistry and petrography of sand sample 09-7A in Appendices 2-4; this sample was collected adjacent to sample WA-47 as part of this study. Petrographic examination of the sands (Appendix 2) shows that they are dominantly composed of monocrystalline quartz-rich with appreciable potassium feldspar, hornblende with some pyroxene, and minor amounts of lithic clasts and polycrystalline quartz grains. Initial TL analyses in 2005-2006 suggested an age of ~200 ka, however the more precise and reliable method of IRSL dating was used to produce ages of $\sim 120 \pm 10$ ka and $\sim 130 \pm 15$ ka (Table 2). The new IRSL age indicates that this nonglacial sediment correlates with the Whidbey Formation.

Table 2. Elemental concentrations, cosmic and total dose rates, equivalent doses and ages from IRSL (fine-grained feldspars); ^a Sample descriptions are only generalized, more detailed descriptions are provided above or in Dragovich and others (2010); ^b Cosmic doses and attenuation with depth were calculated using the methods of Prescott and Hutton (1994); ^c Total dose rate is measured using field moisture, although the full saturation moisture value is shown in parentheses; ^d Reported to one sigma, as are ages; ^f Lab used fine silt grains (5-10 micron size), data fit to an exponential regression and obtained as infrared stimulated luminescence on feldspar by multiple aliquot additive dose. Samples are located on Plate 1 of Dragovich and others (2010). K, % potassium; Gy, Gray (unit of absorbed radiation); ka, 1000 yrs.

Sample no. (geologic unit)	Sediment Type ^a	K (%)	Th (ppm)	U (ppm)	Water Content (%)	Cosmic Dose Rate (Gy/ka) ^b	Total Dose Rate (Gy/ka) ^c	De (Gy) ^d	Age (ka)
09-81Z (unit Qc _o)	silty sand with many silt beds	0.97 ± 0.03	3.92 ± 0.17	1.69 ± 0.10	26 (44)	0.18 ± 0.01	2.11 ± 0.06	99.9 ± 3.30	47.4 ± 2.76 ^f
WA-47 (unit Qc _{ws})	sand with some silt beds	1.11 ± 0.01	2.97 ± 0.23	1.12 ± 0.10	25 (41)	0.07 ± 0.01	1.88 ± 0.08	220 ± 8.8 240 ± 12.3	120 ± 10.9 128 ± 14.1

WHIDBEY FORMATION TEPHROCHRONOLOGY

Introduction and Field Setting

Tephrochronology is a relative dating technique and works by correlating a subject tephra composition to that of a known tephra that has been directly dated by some other technique such as radiocarbon age dating. The premise of the technique is that each volcanic event produces tephra containing glass with a unique chemical "fingerprint" that allows the deposit to be identified across the area affected by fallout. Thus, once the volcanic event has been independently dated, the tephra horizon will act as time-stratigraphic marker. Although an individual tephra can be identified based on its composition as determined by other analytical techniques, it is most commonly done by electron probe microanalysis of the glass component. As is the case in our study, the volcanic glass composition is geochemically determined, not the composition of the volcanic minerals. Tephra are compared with a numeric called a similarity coefficient (or SC; see Borchardt and others, 1972). A similarity coefficient of 0.98 -1.00 indicates a high probability of a match (strong correlation) whereas similarity coefficients <0.88 are not indicative of a match and thus have no geochemical correlation.

Sample 'pumice P' was sampled from a thin bed containing well sorted white pumice lapilli (clasts ~2 cm across) in the Whidbey Formation in southwestern part of the Carnation 7.5-minute quadrangle. The site is adjacent to radiocarbon age site 30E of Dragovich and others (2010) in the NW ¼ of the NW ¼ of Section 25, T25N R6E. Six of the pumice clasts were sent to Washington State University for tephrochronologic analyses. The pumice lapilli clasts are compositionally homogeneous in the field and in thin-section and are composed of scattered microphenocrysts of plagioclase, biotite, hornblende and pyroxene surrounded by clear glass. We obtained an 'infinite' radiocarbon age (>~44 ka) from a peat bed adjacent to the pumice P sample (Appendix 1).

The Whidbey Formation (unit Qc_{wp}) in this area is composed of andesitic cobble gravel, sandy gravel, and gravelly sands with lesser beds of sand and minor silt with plant fossils and rare beds of peat and tephra. The formation in this area is at least 150 feet thick. The spatial association of thin peat, tephra and silt beds suggests deposition as swamp deposits, possibly abandoned fluvial channels. The provenance of the sand and gravel detritus in the Whidbey Formation in the southwestern part of the Carnation quadrangle is the Puget Group southeast of the map area (unit Qc_{wp} of Table 4). This detritus was likely deposited along major drainages (river valleys) emanating from the Seattle uplift as discussed further in Dragovich and others (2010). The volcanic clasts in these deposits are mostly Tukwila Formation andesite and basaltic andesite; less abundant sandstone clasts are arkosic sandstone and are likely mostly from the Renton or

Tiger Mountain Formations. Gravel clasts have weathering characteristics (including mafite rinds 1-2 mm) consistent with the Whidbey Formation. The fluvial Whidbey Formation in this area occurs stratigraphically under Vashon glacial deposits.

Washington State University (WSU) Analysis of Pumice P

Dr. F.F. Foit, Jr. of WSU analyzed the glass in the ‘pumice P’ sample for 9 elements (Table 3) using a JEOL 8500F electron probe microanalyzer. Glass was analyzed from six pumice lapilli and is extremely chemically homogeneous between individual lapilli (Table 3). Dr. Foit maintains a tephra compositional database that we term *WSU tephra compositional database*. The best match to the WSU database for pumice P is to the Rockland tephra (SC = 0.97) which was erupted from Lassen volcano in northern California ~470,000 yrs B.P. However, it is unlikely that pumice P is correlative with the Rockland tephra given the size of the pumice lapilli and the distance to the Lassen volcano. It is also an equally good match (SC = 0.97) to two pumice clasts from the latest Pleistocene Partridge gravel on Whidbey Island which Dr. Foit analyzed for Cynthia Carlstad and tentatively identified as 1.0 Ma Lake Tapps tephra in the 1980’s (Carlstad, 1992). However, as discussed below, because the source for the pumice clasts in the Partridge Gravel is reworked older nonglacial deposits of Olympia (15,000-60,000 yrs B.P.) and Whidbey Formation (80,000-130,000 yrs B.P.) we discount the correlation *directly* with the latest Pleistocene Partridge Gravel. The glass from pumice P has a Glacier Peak compositional signature with a weak similarity (SC=0.94) to the mid-Holocene Glacier Peak Dusty Creek assemblage. Because the Whidbey Formation predates the Holocene age Dusty Creek assemblage, pumice P cannot be correlative with the Holocene Dusty Creek assemblage. However, the weak geochemical similarity with the Dusty Creek assemblage of the Glacier Peak volcano is compelling in light of the likely correlation of pumice P with Glacier Peak pumice samples in the USGS database as discussed below.

Correlation of pumice P with the USGS Database—The Partridge gravel and the Whidbey Formation on Whidbey Island

We contacted Sarna-Wojcicki (USGS retired) who contains a large tephra compositional database which we term the *USGS tephra compositional database*.

CORRELATION WITH THE WHIDBEY FORMATION

Sample DW-98-160 is pumice in the Partridge gravel unit on Whidbey Island (Sarna-Wojcicki, USGS retired, written commun., 2010; Dethier and others, 2005, 2008). Pumice P strongly correlates with DW-98-160 (SC=0.99)—a few elements match exactly but most have similarity coefficients of 0.99 (Table 3). Although the Partridge gravel is a near-ice to ice-contact complex deposited during glacial recession (~11-12 ka) much of the sand and gravel detritus in this complex was derived from sub-glacial fluvial erosion along an ice tunnel and contains much detritus obtained from excavation of older stratigraphic units (Dethier and others, 2008; Dragovich and others, 2005; Polenz and others, 2005). For example, pumice clasts and peat or wood fragments in the Partridge gravel are derived from sub-glacial erosion of the nearby Olympia deposits and Whidbey Formation. Sample DW-98-160 is likely derived from excavation of Glacier Peak lahar runout deposits in the Whidbey Formation as mapped in the Oak Harbor 7.5-minute quadrangle by Dragovich and others (2005) due east of the Partridge unit. An Ar-Ar age date of 128 +/- 9 ka was obtained from pumice or vesicular dacite clasts in the Whidbey Formation on Whidbey Island by Dethier and others (2008). The 128 ka +/- 9 Ar-Ar age correlates reasonably well with the IRLS age for unit Qc_{ws} in the northwestern part of the Carnation quadrangle (Site WA-47, Table 2; 120 ± 10.9 to 128 ± 14.1 ka).

The Whidbey Formation on northern Whidbey Island is ancient Skagit and Stillaguamish River alluvium. This alluvium has a strong Glacier Peak provenance including distinct lahar runout beds from the Glacier Peak volcano (Dragovich and others, 2005). Phenocryst content and whole-rock composition of the dacite clasts in the lahar runout or runouts in the Whidbey Formation strongly suggest a GP source (Dragovich and others, 2005). Given the strong geochemical correlation with DW-98-160 from the Partridge gravel, the weak geochemical similarity with the Dusty Creek assemblage of the Glacier Peak volcano, and the age

correlation between the Ar-Ar pumice within the Whidbey Formation and IRSL date from Site WA-47 in this quadrangle, we conclude that pumice P is correlative with an early Whidbey-age Glacier Peak eruption. Pumice P was obtained from beds that have several characteristics that are similar to the Whidbey Formation regionally, including stratigraphic position, degree of compaction, and weathering characteristics, thus supporting our correlation of unit Qc_{ws} with Whidbey Formation. The apparent widespread nature of the pumice (Carnation area and Whidbey Island), combined with the fact that lahar runout deposits are well-represented in the Whidbey Formation on northern Whidbey Island, may indicate a major voluminous eruptive episode at ~128 ka at Glacier Peak. See caveat discussion below.

A FEW CAVEATS—WHIDBEY FORMATION AND NON-MATCHING SAMPLES

The lahar runout deposits in the Whidbey Formation on Whidbey Island contain abundant semi-vesicular dacite with some scattered pumice clasts. The semi-vesicular dacite clast glass composition of one sample in the lahar run-out deposits does not match pumice P and reportedly no microprobe data exist for Whidbey Formation pumice clasts that match the pumice in the Partridge gravel. For example, compare sample pumice P in Table 4 below and sample D-98-9 reported in Dethier and others (2008) and. We are unsure why the pumice or vesicular dacite from the lahar runout in the Whidbey Formation at Blowers Bluff (Ar-Ar dated to ~130 Ma) does not match pumice P. However, because semi-vesicular dacite dominates in the lahar units in the Whidbey Formation (Dragovich and others, 2005) we suspect that the Ar-Ar sample was a semi-vesicular dacite (not true pumice) common in the lahar runout deposits of the Whidbey Formation on Whidbey Island. Further dating of the individual volcanic clasts in the Whidbey Formation lahar runout deposits might reveal that: (1) some clasts are accidental volcanic fragments that were entrained during lahar runout, (2) the Whidbey Formation on northern Whidbey Island contains lahars from several eruptive episodes, or (3) the semi-vesicular dacite and pumice evolved from the same magmatic source but have a different composition due to magma dynamics such as magmatic segregation. We do however conclude that because clasts having pumice P chemistry have a widespread apparent spatial dispersal (Carnation and Whidbey Island areas) and that thick lahar deposits are present within the Whidbey Formation on northern Whidbey Island (Dragovich and others, 2005), these deposits represent a major voluminous Glacier Peak eruptive event at ~128 ka that produced a significant airfall deposit(s) during Whidbey Formation “time”. However, more work is required to correlate pumice P directly with a Whidbey-age Glacier Peak eruption represented by the dacite and pumice found on Whidbey Island.

Table 3. The composition of glass in pumice P (this study) and sample DW-98-160 (USGS database; Partridge gravel, Whidbey Island). na, not analyzed; *, standard deviations of the analyses given in parentheses; **, analyses normalized to 100 weight percent; ***, number of pumice glass microprobe spots analyzed; ##, similarity coefficient of 0.99 indicates very strong correlation between Pumice P and DW-98-160.

Oxide	Sample Pumice P	Sample DW-98-160	Difference between Pumice P and DW-98-160	Similarity Coefficient Between Pumice P and DW-98-160
SiO ₂	77.65 (0.28)*	77.650 (0.981)	0.00	1.00
Al ₂ O ₃	12.84 (0.18)	12.850 (0.213)	-0.01	1.00
Fe ₂ O ₃	0.87 (0.04)	0.860 (0.058)	0.01	0.99
TiO ₂	0.16 (0.03)	0.160 (0.018)	0.00	1.00
Na ₂ O	3.71 (0.08)	3.750 (0.124)	-0.04	0.99
K ₂ O	3.74 (0.13)	3.760 (0.114)	-0.02	0.99
MgO	0.16 (0.03)	0.160 (0.018)	0.00	1.00
MnO	na	0.020 (0.017)	-	-
CaO	0.77 (0.05)	0.800 (0.048)	-0.03	0.96
Cl	0.10 (0.02)	na	-	-
Total**	100	100.010 (1.153)	-0.01	0.99##
no. of spots***	20	19	1	-
Analyst	Nick Foit, WSU	Sarna-Wojcicki, USGS		

SAND POINT-COUNT DATA—SEDIMENTARY PROVENANCES AND INVERTED BASINS

Dragovich (2007) and Dragovich and others (2009b,c) supply sand point-count data for various Quaternary geologic units including Holocene Snoqualmie River alluvium, Vashon recessional glacial units, Vashon advance outwash and lake deposits, Olympia beds, Whidbey Formation and Possession glacial outwash for the Fall City and Snoqualmie quadrangles. During this study, we visually estimated the percentages of various grain populations for 61 sand thin-section samples from various Quaternary geologic units sampled in the Carnation quadrangle. As shown in Table 4, Quaternary strata in the Snoqualmie Valley area are assigned to four major sedimentary provenances (1) nonglacial Snoqualmie River southeastern source (**SP**), (2) nonglacial local eastern source (**LP**), (3) nonglacial Puget Group northern source (**PG**), and (4) glacial mixed northern source (**GP**) (Dragovich, 2007; Dragovich and others, 2009a,b,c, 2010).

Whidbey Formation, Puget Group provenance sediments (unit Qc_{wp}) are distinct both in the field and in thin section. In the field, unit Qc_{wp} deposits are characterized by compact gravels, cobble gravels and some sand, silt, tephra and peat with moderate weathering. Sands and gravels contain abundant andesitic detritus. Sands in unit Qc_{wp} contain 69-88% clasts (mostly andesite) with some sedimentary clasts (2-8%). Paleocurrent indicators, sedimentary structures and bedding style suggest a northeasterly flowing fluvial (river) source. Because most deposits are quite cobbly, we suspect the river was a high-energy braided river system. The dominance of andesitic (Tukwila Formation) gravel over sedimentary rocks (Renton and Tiger Mountain Formations) is attributed to the resistance of andesite to abrasion; we note here a broadly similar proportion of andesite/sandstone + siltstone + claystone in the modern Raging River, which is similarly sourced by the Puget Group along the Seattle uplift. See Dragovich and others (2010) and Appendices 2-4 for more on the separation of the Whidbey Formation into two distinct sources in the map area: Snoqualmie (unit Qc_{ws}) and Puget Group (unit Qc_{wp}) provenances. Our new mapping (Dragovich and others, 2010) shows that sites 23L and 51Z (mapped as unit Qc_{wp} in Dragovich (2007) in the Carnation quadrangle are actually Whidbey Formation, Puget Group provenance sediments (unit Qc_{wp}). This unit is distinct in the field and in thin section.

Although more fully discussed in previous publications such as Dragovich (2007), modern Snoqualmie River alluvium (unit Qa) is modally similar to ancient Snoqualmie River alluvium such as the Olympia beds (unit Qc_o), as well as part of the Whidbey Formation (unit Qc_{ws}), and these units have a distinct Snoqualmie River SP provenance. We further examined the geochemistry of these provenances during this study (see Sand Geochemistry below). It is likely that the thick SP units (Table 4) locally represent “inverted basins” resulting from strike-slip faulting within the Rattlesnake Mountain fault zone (RMFZ) as discussed in Dragovich and others (2009b,c) for Snoqualmie Ridge to the south of the present map area. In this model, the thick SP alluvium formed in a transtensional basin along the RMFZ. The basin was inverted when the Olympia bed sediments underwent uplift and folding during a later (on-going?) transpressional episode. Similar inverted basins likely occur in the present area such as on Tolt Hill, parts of Union Hill, and perhaps in areas of thick pre-Fraser nonglacial (unit Qc_{pf}) deposits (see ‘inverted basin’ in Figure 4 and ‘Broad Tectonic Features in the Snoqualmie Valley’ below for more information).

Table 4. Major sedimentary provenances for primary Quaternary geologic units in the Carnation, North Bend, Fall City and Snoqualmie 7.5-minute quadrangles. Provenances are defined by compositional data derived from sand point-count data, general petrographic observations, sand geochemistry (discussed below) as well as field data and observations.

Group	Geologic Unit	Provenance	Notes
SP (Snoqualmie Provenance)	Qa (Snoqualmie River), Qc _{os} , Qc _{ws} , Qc _{pf}	Snoqualmie River provenance with generally southeastern fluvial sources; rivers flowing generally northwest along the Rattlesnake Mountain-southern Whidbey Island fault zone (RMFZ-SWIF) over time	Nonglacial units that contain abundant monocrystalline quartz and significant potassium feldspar, plagioclase and minor but distinct granitic lithic grains, biotite and (or) hornblende; major bedrock source is the Snoqualmie Batholith that covers much of the headwaters of the Snoqualmie River. Rivers trapped in RMFZ-SWIF during nonglacial or interglacial intervals.
LP (Local Provenance)	Qa (Tolt River), Qc _{ol}	Local provenance with eastern fluvial sources; rivers flow to the west from the Cascade foothills. Unit Qc _{ol} on Union Hill-Redmond Ridge likely from river tributaries that flowed generally westerly away from the Union Hill anticline	Nonglacial units that contain significant local lithic grains including meta-argillite, volcanic lithic grains, metasandstone; major source is the volcanic rocks of Mount Persis and the Western mélange belt. Sands are typically lithic rich in the eastern part of the Carnation quadrangle. Sands on Union Hill-Redmond Ridge in the western part of the quadrangle have a local composition resulting from the reworking of older glacial and nonglacial deposits. The base of Olympia beds west of the quadrangle is lower in elevation to the west. The beds also thicken substantially to the west suggesting flow away from the Union Hill fold axis.
PG (Puget Group Provenance)	Qc _{wp}	Puget Group provenance with fluvial sources to the south and southwest from the Seattle uplift (for example, Tiger Mountain); rivers flowing north to northeast away from the Seattle uplift and toward the ancient Snoqualmie River	Whidbey Formation (nonglacial) in the southwestern portion of the map area is sourced by the Puget Group and contains significant andesite detritus as well as some arkosic sandstone, siltstone from the Tukwila, Renton and Tiger Mountain Formations. Sands are lithic rich.
GP (Glacial Provenance)	Qgl _r , Qgos, Qgod, Qgof, Qgic, Qgog, Qgt _v , Qga _v , Qgl _v , Qgt _p , Qgo _p , Qgl _p , Qgd _d	Glacial northern provenance locally mixed with some eastern and northeastern Cascade provenance (particularly for some Vashon recessional deposits sourced by ice marginal meltwater); generally southerly flowing glacial meltwater streams, tunnels and proglacial lakes	Glacial units contain variable lithic clasts types including high-grade metamorphic clasts and contain a high polycrystalline/monocrystalline quartz ratio relative to local Cascade sources and lesser potassium feldspar. Sand grains types tend to be polymictic or variable. Figure 1A and 1D shows that Vashon recessional sands have a transitional composition between glacial and nonglacial deposits as a result of local reworking of older sediments during glacial recession.

BEDROCK-TOP CONTOUR MAP

Appendix 5 presents a bedrock-top contour map for the Carnation 7.5-minute quadrangle. This map was compiled using surface mapping, well and boring logs, and published and unpublished depth-to-bedrock information (Jones, 1996; S. Kahle, USGS, written commun., 2009). The main data source was information from 1258 wells, 175 geotechnical borings, and 310 test pits. Gravity and magnetic data was consulted in areas of sparse subsurface data (see queried contacts). Approximate Quaternary-to-Pliocene(?) deposit thickness can be obtained by comparing bedrock-top elevations with the Snoqualmie topographic base map or cross sections on Plate 1 of Dragovich and others (2010). The top of bedrock is locally ambiguous in some water well reports. For example, below Union Hill some water wells report bedrock lithologies (for example, sandstone) interbedded with apparent unconsolidated deposits (for example, gravel). Because Miocene and some Oligocene strata in the area are only poorly to moderately lithified, and thus may react to drilling similarly to compact Quaternary deposits, we typically map the top of bedrock at the highest

reported elevation of a bedrock lithology (see queried bedrock top contours below the Union Hill anticline on the bedrock-top map in Appendix 5). Some structural and geomorphic observations of the bedrock-top contour map include:

- Portions of the proposed Tolt Hill and Union Hill anticlines are associated with ridges of bedrock. These arching bedrock highs may be the result of Quaternary growth folding particularly in areas where the apparent bedrock uplift is coincident with mapped Quaternary folds (see ‘unconsolidated deposit bedding’ on Plate 1 of Dragovich and others, 2010, and ‘Tolt Hill anticline’ in Dragovich and others, 2007). Some bedrock top slopes may be dip slopes especially where the slope of the bedrock top approximates the inferred bedrock bedding dip angle (compare Cross Sections A and B in Dragovich and others, 2010, with bedrock-top map, Appendix 5).
- Some steeply sloping and (or) high bedrock escarpments are spatially coincident with some mapped faults segments in the study area, including segments of Snoqualmie Valley fault no. 1, Rattlesnake Mountain fault no. 1, and the Cherry Creek fault.
- Although speculative, closely spaced bedrock-top data reveal what appear to be linear bedrock-top features that may define ancient channels of the Snoqualmie River. If they exist, most of these channels were scoured prior to deposition of the Whidbey Formation and thus are mid-to-early Pleistocene in age.

U-PB LA-ICP-MS GEOCHRONOLOGY

Introduction and Sample Description

We obtained a uranium-lead (U-Pb) age from a lapilli tuff as part of our Carnation quadrangle geologic mapping effort. Relative probability plots versus age plots and age are supplied in Appendix 6 (see Table 1 for appendix file names).

Pebbly sandstones and lithic vitric lapilli tuff are exposed in scattered outcrops on the Maltby 7.5-minute quadrangle about 1,000-2,000 ft directly north of the northwest corner of the Carnation quadrangle on the Snoqualmie Valley Road (Dragovich and others, 2010). The internal structure and relative distribution of these outcroppings suggests that a very thick bed of lapilli tuff is interbedded with stratified sandstone and pebbly sandstone. The lapilli tuff outcrops were targets for U-Pb geochronology because of their isolation from other bedrock outcroppings and critical position within the southern Whidbey Island fault zone. We initially suspected (on the basis of composition, degree of lithification, and previous mapping by Minard, 1985) that these rocks are correlative with the Blakeley Formation. New data suggests that the rocks are the Miocene volcanic rocks of Snoqualmie Falls or the uppermost part of the Blakeley Formation as discussed below.

Methods

Zircons for this study were analyzed for U and Pb isotopes using laser ablation inductively coupled mass spectrometry (LA-ICP-MS) at the University of Alberta Radiogenic Isotope Facility (RIF). A full description of the analytical approach is reported in Simonetti and others (2005). A brief description is provided below.

ZIRCON SEPARATION

Each sample (~10-15 kg) was crushed to fine sand-sized particles. Heavy minerals were then concentrated using a Wilfley table. Between each sample, great care was taken to clean crushing plates and the Wilfley table to reduce the risk of contamination. The zircon concentrate was then passed through a 350 mm sieve and the < 350 mm fraction was cleaned by magnetic separation using a Frantz LB1. Zircons were then separated by density from the non-magnetic fraction using methylene iodide heavy liquid. From the zircon separate, ~10-50 individual zircon grains were selected from each sample and mounted in epoxy. The grain

mount was polished to expose the grain centers. Regions suitable for analysis were identified from optical imaging.

LA-ICP-MS

The analytical setup at the RIF consists of a New Wave UP-213 laser ablation system interfaced with a Nu plasma multi-collector inductively coupled plasma mass spectrometer (MC-ICPMS) equipped with three ion counters. We operated the laser at 4 Hz repetition rate at a fluence of $\sim 3 \text{ J/cm}^2$. Laser beam size was 30 mm and pit depth was 25 mm for a typical analysis. Data were collected statically, consisting of 30 1s integrations. Prior to and during each analytical session, zircon reference material GJ1 was analyzed repeatedly and was used to normalize the unknowns, thus correcting for U-Pb fractionation and instrument drift. Mass bias for Pb isotopes was corrected by simultaneously aspirating a 1 ppb Tl solution.

DATA REDUCTION AND UNCERTAINTIES

All data were reduced offline using an Excel-based program. The uncertainties reported here are a quadratic combination of: 1) the standard error of the measured $^{206}\text{Pb}/^{238}\text{U}$, and 2) the standard deviation in the $^{206}\text{Pb}/^{238}\text{U}$ determinations of the standards that bracket the unknowns. Overall uncertainty in age is conservatively estimated to be between 3 and 5% (1 sigma). No common Pb correction was performed on any of the analyses reported here due to the young age of the sample and the uncertainties associated with subtracting the ^{204}Hg background.

Further Information and Interpretation

We obtained a tentative $^{206}\text{Pb}/^{238}\text{U}$ zircon age of 16 to 20 Ma ($\sim 18 \text{ Ma}$) from sample 09-54Z (Appendix 6). The age is considered preliminary because of the analytical uncertainty associated with $\text{Pb}^{207}/\text{Pb}^{206}$ ratios due to low counts on Pb^{207} , often resulting in negative numbers. This uncertainty is a direct result of the young age of the deposit. The age is derived from the youngest zircon (18 Ma) in the zircon age population and is interpreted to reflect the deposition of this pyroclastic deposit. The older zircons measured were likely incorporated into the parent magma during intrusion or derived from pyroclastic deposits during extrusion and catastrophic dispersal as discussed below.

Pebbly sandstones and lithic vitric lapilli tuff are exposed 1,000 to 2,000 ft directly north of the northwest corner of the Carnation quadrangle on the Snoqualmie Valley Road (Dragovich and others, 2010). The brown-gray pebbly sandstones are very thickly bedded and contain about 95 to 98 percent subrounded andesite clasts with a few plagioclase, polycrystalline quartz, and greenstone clasts, and are probably fluvial deposits or volcanic hyperconcentrated flood deposits. The dark gray-green lapilli tuff is composed of andesite ($\sim 40\%$), plagioclase ($\sim 20\%$), pumice ($\sim 10\%$), and a few scattered exotic grains of polycrystalline quartz and sedimentary lithic grains set in a matrix of volcanic glass. The poor sorting, angularity of most grains, high proportion of volcanic clasts, and glassy matrix suggests deposition of the tuff as a pyroclastic flow. The bedding style of the sandstones and pebbly sandstones near the poorly exposed pyroclastic deposits suggests deposition in a fluvial or deltaic setting.

The age indicates the sample is Miocene and, given the pyroclastic nature of the deposit, likely a distal equivalent of the volcanic rocks of Snoqualmie Falls of Dragovich and others (unit Mva₃; 2009b,c) mapped in the Snoqualmie quadrangle south-southeast of the sample site. Dragovich and others (2009a) previously obtained a U-Pb zircon age of $22.26 \pm 0.57 \text{ Ma}$ from an andesite flow near the base of Snoqualmie Falls (age site 07-23A, Fig. 1, Appendix A in Dragovich and others, 2009a). Dragovich and others (2009b,c) obtained two additional U-Pb zircon ages from andesite flows along the periphery of the volcanic complex: $18.25 \pm 0.43 \text{ Ma}$ (age site 08-57B, 1.5 mi downriver from Snoqualmie Falls) and $22.76 \pm 0.33 \text{ Ma}$ (age site 08-44C, on Tokul Creek a few miles east of Snoqualmie Falls). These age sites are located on Plate 1 of Dragovich and others (2009b). Thus the apparent age range for the volcanic rocks of Snoqualmie Falls is $\sim 18\text{--}23 \text{ Ma}$. Because the youngest part of the Blakeley Formation is now thought to be earliest Miocene in age (Prothero and Nesbitt, 2008) the deposit was initially interpreted to be part of the uppermost Blakeley Formation; however the 18 Ma age is likely younger than the uppermost Blakeley which is as young as ~ 22

Ma (E. Nesbitt, UW, written commun., 2010). Therefore, these deposits are likely somewhat younger than the nonmarine equivalent of the Blakeley Formation or unit OEc of Dragovich and others (2010). The Blakeley may correlate with the rocks of Bulson Creek (Marcus, 1981) in Skagit County north of the study area (Yount and Gower, 1991), which have a similar fluvial to marine depositional setting.

The Oligocene, Eocene and mid-Cretaceous zircons obtained from the lapilli tuff and the early Oligocene, Eocene, Cretaceous, and Jurassic zircons are likely assimilated accidental zircons incorporated during both magmatic ascent and later pyroclastic dispersal from the edifice near Snoqualmie Falls. The ages of the older 'accidental' zircons compare favorably with the ages of older zircons in the volcanic rocks of Snoqualmie Falls which generally contain Oligocene, Eocene and mid-Cretaceous zircons as well as a few mid-Jurassic zircons. (Compare Appendix 2 of Dragovich and other [2009c] with Appendix 6 [this study]). Candidates for assimilated underlying geologic units include rocks of the Cretaceous to Jurassic Western mélange belt, Oligocene-Eocene Blakeley Formation or perhaps the Eocene volcanic rocks of Mount Persis or the Eocene Puget Group (Dragovich and others, 2009a,b,c, 2010; Tabor and others, 1993). We suspect that: (1) the scattered white pumice in the deposit is the primary volcanic material for the sample; and (2) the much denser intermediate composition clasts are volcanic detritus excavated from the edifice or incorporated during pyroclastic dispersal. The spread of single-zircon U-Pb ages is consistent with the variety of volcanic lithic grain types in the sample. Our suspicion that the pumice in the deposit is the primary juvenile material for the deposit could be confirmed by directly dating only the pumice clasts in the deposit. The general lack of basement rock types in the pyroclastic deposits (rare polycrystalline clasts might be pre-Tertiary metachert grains) suggests the older zircons in the sample were assimilated into the magma from the country rock during parent magma ascent.

Structurally, these Miocene rocks occur between Rattlesnake Mountain fault no.1 and Snoqualmie Valley fault nos. 2 and 3 and would structurally project to unit Mvc shown in the middle of stratigraphic Cross Section A of Dragovich and others (2010) and the corresponding geophysical cross section in this document (Figure 2B). Unit Mvc along this cross section, and probably around the sample site northwest of the section, is apparently preserved in a structural basin within the RMFZ. Note the occurrence of the Blakeley Formation, Puget Group, volcanic rocks of Mount Persis and Western mélange belt stratigraphically below unit Mvc on the various cross sections.

GEOCHEMISTRY OF QUATERNARY SAND DEPOSITS AND THE VOLCANIC ROCKS OF MOUNT PERSIS

Introduction and Methods

New whole rock major and trace elements for 42 glacial and nonglacial sands, and three samples from the volcanic rocks of Mount Persis of Tabor and others (1993), were determined by X-ray fluorescence (XRF) and inductively coupled plasma source mass spectrometer (ICP-MS) at the Geoanalytical Laboratory at Washington State University (WSU).

Grinding of samples for XRF and ICP-MS analyses was done at WSU, using tungsten carbide mill and iron equipment respectively (Johnson and others, 1999). Estimates of accuracy and precision for both XRF and ICP-MS at WSU are given by Johnson and others (1999) and Knaack and others (1994) respectively. See Johnson and others (1999) and Knaack and others (1994) for discussion of analytical methods. Before grinding, all 42 Quaternary sediments were sieved with 2 and 0.075 mm sieves at the DNR laboratory in Olympia so that only the sand-sized fraction was chemically analyzed. This was done to eliminate erroneous results that may occur from large gravel-sized clasts and to remove the variable amounts of silt and clay from these sandy samples. Using this technique, we provide a better comparison between the glacially and nonglacially derived sediments by assuring that we are only comparing the composition of the sands rather than comparing sands with silty sands or sandy silts.

Geochemical data for one Holocene alluvium sand sample and one Olympia Bed sand sample from the adjacent Fall City 7.5-minute quadrangle (Dragovich, 2007) are also included in the sand geochemical

database. We also include geochemical data for one flow and two vitric tuffs from the Eocene volcanic rocks of Mount Persis of Tabor and others (1993) from the adjacent Snoqualmie 7.5-minute quadrangle (Dragovich and others, 2009b,c). The geochemical data, sample petrography, and other sample information are supplied as an electronic attachment (Appendix 2). Additionally, the locations of the geochemical samples for the Carnation quadrangle are provided in Appendix 3. Finally, the geochemical plots (figures cited below) are supplied in a Portable Document Format (PDF) file attachment (Appendix 4) as well as Figures 1A-1D below. See Dragovich and others (2010) for geologic symbols for the Carnation quadrangle bedrock geologic units cited below. For example, Evbx_p is the symbol for the Eocene volcanic breccia from the volcanic rocks of Mount Persis of Tabor and others (1993).

Quaternary Sand Geochemistry

Major- and trace-element geochemistry of sediments can provide invaluable information about their original tectonic setting and provenance (Roser and Korsch, 1986; McLennan and others, 1993). Biogenic CaCO₃ or SiO₂, high concentrations of heavy minerals or quartz, as well as diagenetic reactions related to burial can affect the concentrations of elements within a sedimentary sample (Galloway, 1974; Roser and Korsch, 1986, 1988; McLennan, 1989). Thus, caution should be used when making interpretations based on geochemical analyses of sediments, and ratios should be used whenever possible. Typically, sediments are plotted and interpreted on a CaO-free basis, because dilution resulting from CaCO₃ cannot be corrected without knowing CO₂ values (Roser and Korsch, 1986, 1988); however, petrography of the Quaternary sands indicate that they lack CaCO₃ (Appendix 2; Table 4), thus there was no need to normalize our data CaO-free as all calcium must be coming from non-carbonate minerals.

HOLOCENE NONGLACIAL DEPOSITS

Alluvium (unit Qa)—Four alluvium sands, including one sample from the Fall City 7.5-minute quadrangle (Dragovich, 2007), have chondrite-normalized La/Lu ratios between 4.8 and 6, and Zr between 97 and 134 parts per million (ppm) (Fig. 1A). These same sands plot within the intermediate igneous provenance field on the Roser and Korsch (1988) provenance discriminant function diagram (Fig. 1B). These sands have SiO₂, in weight percentage (wt%), between 70 and 73; CaO+Na₂O between 5.7 and 6.4 wt%; Al₂O₃ between 13.5 and 14.5 wt%; TiO₂ between 0.52 and 0.65 wt%; and, FeO^T+MgO between 5.8 and 6.5 wt% (Appendix 4, Fig. 1). The Th/Sc ratios for these sands range between 0.17 and 0.28 and their Pb is between 6.8 and 8.05 ppm (Appendix 4, Fig. 2). On the Th-Sc-Zr/10 sandstone tectonic discrimination diagram of Bhatia and Crook (1986), these sands plot within or near the field for island arcs (Appendix 4, Fig. 3); while they predominantly plot within the continental arc field, with one sample plotting in the overlap with active continental margins, on the Al₂O₃/SiO₂ vs. Fe₂O₃^T+MgO sandstone tectonic discriminant diagram of Bhatia, 1983 (Appendix 4, Fig. 4).

PLEISTOCENE GLACIAL AND NONGLACIAL DEPOSITS

Deposits of the Fraser Glaciation

Outwash sand (unit Qgos)—One sand from this unit has a chondrite-normalized La/Lu ratio of ~4.6 and Zr of 94 ppm (Fig. 1a). This sample plots within the intermediate igneous provenance field on the Roser and Korsch (1988) provenance discriminant function diagram (Fig. 1B). It has SiO₂ of 73.91 wt%; CaO+Na₂O of 5.75 wt%; Al₂O₃ of 12.46 wt%; TiO₂ of 0.55 wt%; and, FeO^T+MgO of 6.03 wt% (Appendix 4, Fig. 1). The Th/Sc ratio for this sample is ~0.19 and has Pb of 5.13 ppm (Appendix 4, Fig. 2). On the Th-Sc-Zr/10 sandstone tectonic discrimination diagram of Bhatia and Crook (1986), this sample plots within the field for island arcs (Appendix 4, Fig. 3); while it plots near the overlap between active continental margins and continental arcs on the Al₂O₃/SiO₂ vs. Fe₂O₃^T+MgO sandstone tectonic discriminant diagram of Bhatia, 1983 (Appendix 4, Fig. 4).

Deltaic outwash and kame deltas (unit Qgod)—One sand from this unit has a chondrite-normalized La/Lu ratio of approximately 4.16 and Zr of 92 ppm (Fig. 1a). This sample plots within the intermediate igneous provenance field on the Roser and Korsch (1988) provenance discriminant function diagram (Fig. 1B). It

has SiO_2 of approximately 73.27 wt%; $\text{CaO}+\text{Na}_2\text{O}$ of approximately 5.82 wt%; Al_2O_3 of approximately 12.85 wt%; TiO_2 of approximately 0.52 wt%; and, $\text{FeO}^{\text{T}}+\text{MgO}$ of approximately 6.20 wt% (Appendix 4, Fig. 1). The Th/Sc ratio for this sample is ~ 0.18 and Pb of ~ 4.68 ppm (Appendix 4, Fig. 2). On the Th-Sc-Zr/10 sandstone tectonic discrimination diagram of Bhatia and Crook (1986), this sand plots within the field for island arcs (Appendix 4, Fig. 3); also, this sand plots within the overlap between active continental margins and continental arcs on the $\text{Al}_2\text{O}_3/\text{SiO}_2$ vs. $\text{Fe}_2\text{O}_3^{\text{T}}+\text{MgO}$ sandstone tectonic discriminant diagram of Bhatia, 1983 (Appendix 4, Fig. 4).

Ice-contact kames and kame deltas (unit Qgik) — Three samples from this unit have chondrite-normalized La/Lu ratios that range from 4.06 to 5.29 and Zr values that range from 84 to 92 ppm (Fig. 1A). Two of these sands plot within the intermediate igneous provenance field on the Roser and Korsch (1988) provenance discriminant function diagram, while sand 7B plots within the field for mafic igneous provenance (Fig. 1B). The SiO_2 contents for these sands range from 72.13 to 75.84 wt%; their $\text{CaO}+\text{Na}_2\text{O}$ contents range from 4.95 to 6.58 wt%; Al_2O_3 from 11.65 to 13.24 wt%; TiO_2 from 0.51 to 0.59 wt%; and, their $\text{FeO}^{\text{T}}+\text{MgO}$ contents range from 5.42 to 6.72 wt% (Appendix 4, Fig. 1). The Th/Sc ratios for these samples range from 0.16 to 0.20 and their Pb contents range from 4.60 to 5.59 ppm (Appendix 4, Fig. 2). On the Th-Sc-Zr/10 sandstone tectonic discrimination diagram of Bhatia and Crook (1986), all three of these samples plot within the field for island arcs (Appendix 4, Fig. 3). Sample 6Q plots near the field for active continental margins, sample 32R plots within active continental margins field and 7B plots near the overlap between active continental margins and continental arcs on the $\text{Al}_2\text{O}_3/\text{SiO}_2$ vs. $\text{Fe}_2\text{O}_3^{\text{T}}+\text{MgO}$ sandstone tectonic discriminant diagram of Bhatia, 1983 (Appendix 4, Fig. 4).

Vashon advance outwash (unit Qga_v) — One sand from this unit has a chondrite-normalized La/Lu ratio of approximately 3.93 and Zr of approximately 81 (Fig. 1A). This sand plots within the intermediate igneous provenance field on the Roser and Korsch (1988) provenance discriminant function diagram (Fig. 1B). It has SiO_2 of ~ 73.65 wt%; $\text{CaO}+\text{Na}_2\text{O}$ of ~ 5.15 wt%; Al_2O_3 of ~ 13.76 wt%; TiO_2 of ~ 0.50 wt%; and, $\text{FeO}^{\text{T}}+\text{MgO}$ of ~ 5.16 wt% (Appendix 4, Fig. 1). The Th/Sc ratio for this sample is ~ 0.16 and it has Pb of ~ 4.88 ppm (Appendix 4, Fig. 2). On the Th-Sc-Zr/10 sandstone tectonic discrimination diagram of Bhatia and Crook (1986), this sand plots within the field for island arcs (Appendix 4, Fig. 3). This sand plots within the overlap between active continental margins and continental arcs on the $\text{Al}_2\text{O}_3/\text{SiO}_2$ vs. $\text{Fe}_2\text{O}_3^{\text{T}}+\text{MgO}$ sandstone tectonic discriminant diagram of Bhatia, 1983 (Appendix 4, Fig. 4).

Deposits of the Olympia Nonglacial Interval (Olympia Beds)

Olympia beds of Minard and Booth (1988)(units Qc_o and Qc_{ol}) — Fifteen samples from these two units (fourteen from Qc_o and one, 31R, from Qc_{ol}) have chondrite-normalized La/Lu ratios that range from approximately 3.80 to 5.85 and Zr from approximately 64 to 112 ppm (Fig. 1A). These sands plot within the intermediate igneous provenance field on the Roser and Korsch (1988) provenance discriminant function diagram (Fig. 1b). These samples have SiO_2 contents that range between 70.99 and 76.37 wt%; $\text{CaO}+\text{Na}_2\text{O}$ that range between 5.24 and 6.54 wt%; Al_2O_3 between 11.08 and 14.43 wt%; TiO_2 between 0.42 and 0.62 wt%; and, $\text{FeO}^{\text{T}}+\text{MgO}$ contents that range between 4.71 and 6.82 wt% (Appendix 4, Fig. 1). These sands have Th/Sc ratios that range from 0.16 to 0.30 and Pb values from 4.16 to 7.44 ppm (Appendix 4, Fig. 2). Fourteen of these sands plot within the field for island arcs, and sample 10C plots within the overlap between island and continental arcs on the Th-Sc-Zr/10 sandstone tectonic discrimination diagram of Bhatia and Crook, 1986 (Appendix 4, Fig. 3). On the $\text{Al}_2\text{O}_3/\text{SiO}_2$ vs. $\text{Fe}_2\text{O}_3^{\text{T}}+\text{MgO}$ sandstone tectonic discriminant diagram of Bhatia (1983) six sands plot within or around the active continental margin field, six sands plot within or near the overlap between active continental margins and continental arcs, and three sands plot within or near the field for continental arcs (Appendix 4, Fig. 4).

Deposits of the Possession Glaciation

Outwash (unit Qgo_p) — Two sands from this unit have chondrite-normalized La/Lu ratios that range from 3.57 to 4.16 and Zr that range from 83 to 94 ppm (Fig. 1a). These sands plot within the intermediate igneous provenance field on the Roser and Korsch (1988) provenance discriminant function diagram (Fig. 1b). These sands have SiO_2 contents that range between 74.86 and 75.08 wt%; $\text{CaO}+\text{Na}_2\text{O}$ that range between 4.89 and 5.05 wt%; Al_2O_3 between 12.09 and 12.38 wt%; TiO_2 between 0.51 and 0.59 wt%; and,

$\text{FeO}^{\text{T}}+\text{MgO}$ contents that range between 5.94 and 6.15 wt% (Appendix 4, Fig. 1). Their Th/Sc ratios range between 0.16 and 0.20 and their Pb contents range between 4.65 and 4.98 ppm (Appendix 4, Fig. 2). These samples plot within the island arc field on the Th-Sc-Zr/10 sandstone tectonic discrimination diagram of Bhatia and Crook, 1986 (Appendix 4, Fig. 3). On the $\text{Al}_2\text{O}_3/\text{SiO}_2$ vs. $\text{Fe}_2\text{O}_3^{\text{T}}+\text{MgO}$ sandstone tectonic discriminant diagram of Bhatia (1983) these samples plot near the field for active continental margins (Appendix 4, Fig. 4).

Whidbey Formation

Whidbey Formation, Puget Group Formation provenance (unit Qc_{wp}) — Five samples from this unit have chondrite-normalized La/Lu ratios that range from 4.89 to 6.51 and Zr contents that range from 113 to 141 ppm (Fig. 1a). Three of these sands plot within the intermediate igneous provenance field on the Roser and Korsch (1988) provenance discriminant function diagram; while two samples (30H and 38G; Appendix 2) plot within the mafic igneous provenance field on this diagram (Fig. 1B) consistent with their andesite-clast rich nature. These sands have SiO_2 contents that range between 64.00 and 76.79 wt%; $\text{CaO}+\text{Na}_2\text{O}$ between 5.03 and 7.61 wt%; Al_2O_3 between 11.26 and 16.93 wt%; TiO_2 between 0.38 and 0.90 wt%; and, $\text{FeO}^{\text{T}}+\text{MgO}$ contents that range between 5.12 and 9.24 wt% (Appendix 4, Fig. 1). They have Th/Sc ratios that range between 0.16 and 0.35 and their Pb contents range from 4.09 to 7.14 ppm (Appendix 4, Fig. 2). Two of these samples plot within the field for island arcs, one sample (30C) plots within the field for continental arcs, and two samples (11V and 30H) plot near the overlap between island and continental arcs on the Th-Sc-Zr/10 sandstone tectonic discrimination diagram of Bhatia and Crook, 1986 (Appendix 4, Fig. 3). On the $\text{Al}_2\text{O}_3/\text{SiO}_2$ vs. $\text{Fe}_2\text{O}_3^{\text{T}}+\text{MgO}$ sandstone tectonic discriminant diagram of Bhatia (1983) two sands (samples 11V and 30C) plot within the active continental margin field, one sample (11B) plots within the field for continental arcs, and two samples (30H and 38G) plot within or around the field for oceanic arcs (Appendix 4, Fig. 4).

Whidbey Formation, Snoqualmie River provenance (unit Qc_{ws}) — Five sands from this unit have chondrite-normalized La/Lu ratios that range from 4.29 to 5.69 and Zr contents that range from 105 to 156 ppm (Fig. 1A). Four of these sands plot within the intermediate igneous provenance field, while one sand (sample 7A) plots within the mafic igneous provenance field on the Roser and Korsch (1988) provenance discriminant function diagram (Fig. 1B). These sands have SiO_2 contents that range from 73.48 to 75.74 wt%; $\text{CaO}+\text{Na}_2\text{O}$ from 4.89 to 5.74 wt%; Al_2O_3 from 11.35 to 13.81 wt%; TiO_2 from 0.48 and 0.61 wt%; and, $\text{FeO}^{\text{T}}+\text{MgO}$ contents that range from 5.17 and 6.71 wt% (Appendix 4, Fig. 1). Their Th/Sc ratios range from 0.22 to 0.27 and their Pb contents range from 6.25 to 7.28 ppm (Appendix 4, Fig. 2). On the Th-Sc-Zr/10 sandstone tectonic discrimination diagram of Bhatia and Crook (1986) one sample (39L) plots within the island arc field, two samples (25C and 25E) plot near the overlap between island and continental arcs, and two samples (7A and 25A) plot near the field for continental arcs (Appendix 4, Fig. 3). One sand (sample 25E) plots within the active continental margins field and the others plot near the overlap between continental arcs and active continental margins on the $\text{Al}_2\text{O}_3/\text{SiO}_2$ vs. $\text{Fe}_2\text{O}_3^{\text{T}}+\text{MgO}$ sandstone tectonic discriminant diagram of Bhatia, 1983 (Appendix 4, Fig. 4).

Double Bluff Drift

Double Bluff drift (unit Qgd_d) — Two sands from this unit have chondrite-normalized La/Lu ratios that range from 3.47 to 3.87 and Zr contents that range from 93 to 117 ppm (Fig. 1A). These sands plot within the intermediate igneous provenance field on the Roser and Korsch (1988) provenance discriminant function diagram (Fig. 1B). They have SiO_2 contents that range from 73.82 to 75.76 wt%; $\text{CaO}+\text{Na}_2\text{O}$ from 5.41 to 5.72 wt%; Al_2O_3 from 11.62 to 12.24 wt%; TiO_2 between 0.54 and 0.66 wt%; and $\text{FeO}^{\text{T}}+\text{MgO}$ contents that range from 5.59 to 6.30 wt% (Appendix 4, Fig. 1). Their Th/Sc ratios range between 0.18 and 0.20 and their Pb contents range between 4.94 and 5.03 ppm (Appendix 4, Fig. 2). On the Th-Sc-Zr/10 sandstone tectonic discrimination diagram of Bhatia and Crook (1986) these two sands plot within the field for island arcs (Appendix 4, Fig. 3). On the $\text{Al}_2\text{O}_3/\text{SiO}_2$ vs. $\text{Fe}_2\text{O}_3^{\text{T}}+\text{MgO}$ sandstone tectonic discriminant diagram of Bhatia (1983) one sand (sample 24B) plots near the field for active continental margins and the other (sample 24K) plots near the overlap between continental arcs and active continental margins (Appendix 4, Fig. 4).

Pre-Fraser Glacial And Nonglacial Deposits Undivided

Continental nonglacial deposits (pre-Fraser) (unit Qc_{pf}) — Five samples from this unit have chondrite-normalized La/Lu ratios that range between 4.77 and 5.60 and Zr contents that range from 79 to 155 ppm (Fig. 1A). On the Roser and Korsch (1988) provenance discriminant function diagram three of these sands plot within the intermediate igneous provenance field while two samples (37D and 43G-1) plot within the mafic igneous provenance field (Fig. 1B). The SiO_2 contents for these samples range from 61.58 to 74.31 wt%; $CaO+Na_2O$ between 5.86 and 6.63 wt%; Al_2O_3 from 12.10 to 20.88 wt%; TiO_2 between 0.47 and 0.88 wt%; and FeO^T+MgO contents range between 5.93 and 9.43 wt% (Appendix 4, Fig. 1). The Th/Sc ratios of these six samples range between 0.17 and 0.24 and their Pb contents range from 4.78 to 9.60 ppm (Appendix 4, Fig. 2). On the Th-Sc-Zr/10 sandstone tectonic discrimination diagram of Bhatia and Crook (1986) three sands (samples 37D, 43G-1, and 43H) plot within the field for island arcs, while the other two sands plot near the overlap between island and continental arcs (Appendix 4, Fig. 3). On the Al_2O_3/SiO_2 vs. $Fe_2O_3^T+MgO$ sandstone tectonic discriminant diagram of Bhatia (1983) one sand (43H) plots near the field for active continental margins, two samples plot within and one sample plots near the continental arc field, and one sample (37D) plots near the field for oceanic arcs (Appendix 4, Fig. 4).

Quaternary Sand Geochemistry—General Findings

In general, most of the sands chemically analyzed from the Carnation 7.5-minute quadrangle plot within the intermediate igneous provenance field on the Roser and Korsch (1988) provenance discriminant function diagram (Fig. 1B). These sands plot predominantly within the island arc field, with some overlapping the continental arc field, on the Th-Sc-Zr/10 sandstone tectonic discrimination diagram of Bhatia and Crook, 1986 (Appendix 4, Fig. 3). Also, they plot within the fields for continental arcs and active continental margins on the Al_2O_3/SiO_2 vs. $Fe_2O_3^T+MgO$ sandstone tectonic discriminant diagram of Bhatia, 1983 (Appendix 4, Fig. 4). This suggests that these sands are predominantly derived from an intermediate arc source with minor recycled terrigenous components. This is supported by the low chondrite-normalized La/Lu ratios, moderate Zr (Fig. 1a), Th/Sc ratios much less than 1, and generally moderate Pb (Appendix 4, Fig. 2) (Floyd and others, 1991; McLennan and others, 1990, 1993; McDonough and Sun, 1995; McLennan, 2001). The SiO_2 contents for these sands tend to plot higher than intermediate compositions; however, this is attributed to the concentration of silicates after sieving the samples to remove the silts and clay fraction. The sand petrography (Appendix 2) and provenance (Table 4) corroborate these interpretations.

Figure 1B shows that six samples (two each from units Qc_{wp} and Qc_{pf} and one each from Qc_{ws} and $Qgik$) plot within the mafic igneous provenance field on the Roser and Korsch (1988) provenance discriminant function diagram. Unit Qc_{wp} (samples 30H and 38G) and unit Qc_{pf} (samples 37D and 43G-1) samples also have higher $CaO+Na_2O$, Al_2O_3 , TiO_2 , and FeO^T+MgO , and lower SiO_2 than all other sands (Appendix 4, Fig. 1). Three of these samples plot close to the oceanic arc field on the Al_2O_3/SiO_2 vs. $Fe_2O_3^T+MgO$ sandstone tectonic discriminant diagram of Bhatia, 1983 (Appendix 4, Fig. 4). This suggests that these samples are more intermediate than all other sands with the higher $CaO+Na_2O$ and Al_2O_3 originating from plagioclase, whereas TiO_2 and FeO^T+MgO are originating from volcanically derived ferromagnesian minerals. The sand petrography (Appendix 2) and provenance (Table 4) corroborate these interpretations.

Geochemical Discrimination of Glacial Versus Nonglacial Sand Deposits

Mahoney and others (2003), Saltonstall and others (2003), and Mahoney (2007) have all had moderate success geochemically distinguishing glacial and nonglacial Quaternary sediments in the region. Utilizing similar elemental discriminants, we are also generally discriminating between glacial and nonglacial deposits. The glacially-derived sands tend to have lower chondrite-normalized La/Lu ratios than the nonglacial sands (Figs. 1A and 1D). This may indicate that the glacially derived sands originated from a provenance that was not as enriched as the nonglacially derived sands (McDonough and Sun, 1995). The glacially derived sands generally have lower Zr than the nonglacially derived sands (Fig. 1a). Zr is concentrated in the heavy mineral zircon, which originates in felsic to intermediate igneous rocks, and can

become concentrated by the transportation and recycling of sediments (McLennan, 1989; McLennan and others, 1993). The glacially derived sands have slightly lower Th/Sc ratios than the nonglacially derived sands (Appendix 4, Fig. 2). This suggests that the nonglacially derived sands originated from a slightly more felsic source than the glacially derived sands (Floyd and others, 1991; McLennan and others, 1993) consistent with an SP source (Table 4) for many of the nonglacial sands. The nonglacially derived sands generally have higher Pb than the glacially derived sands (Appendix 4, Fig. 2). Pb is much higher in felsic rocks and upper continental crust (McLennan, 2001), thus the nonglacially derived sands may have a slightly more felsic source. The geochemical differences outlined above suggests that the nonglacially derived sands originated from a slightly more felsic igneous source and (or) were transported farther than the glacially derived sands. Also, the higher $\text{CaO}+\text{Na}_2\text{O}$ and Al_2O_3 contents in the nonglacially derived sands suggest that they are richer in feldspar than the glacially derived sands; while the higher TiO_2 and $\text{FeO}^{\text{T}}+\text{MgO}$ contents suggest that the nonglacially derived sands have more ferromagnesian minerals, such as biotite and hornblende, than the glacially derived sands (Appendix 4, Fig. 1). These findings are supported by the sand petrography (Appendix 2) and provenance (Table 4). For example, Snoqualmie provenance Olympia beds have a strong Snoqualmie batholith granite and granodiorite source and have slightly more plagioclase and significantly more potassium feldspar as well as more hornblende and biotite than glacial deposits (Dragovich, 2007; Dragovich and others, 2007, 2009a,b,c).

Glacial samples 7B and 32R, from unit Qgik, and 35S, from unit Qgos, plot closer to nonglacially derived sands than the other glacially derived sands on many plots (Fig. 1A and 1D; Appendix 4, Fig. 1 and Fig. 2). Glacial sand sample 7B is a kame deposit that was partially derived via meltwater erosion from the nonglacial Whidbey Formation (Qc_w) that sits directly below the kame (Appendix 2). Similarly, sample 32R is also kame sand that may have been partially derived from the Olympia beds (Appendix 2). Glacial outwash sand (sample 35S) was similarly partially derived directly from excavation of the underlying Olympia beds (Qc_o , Appendix 2). The origin of these glacial sands partially from excavation of older nonglacial sands can account for their positions on several of the diagrams midway between glacial and nonglacial sediments (Fig. 1A and 1D).

We can distinguish between *Snoqualmie*, *Local*, and *Puget Group* provenances using petrography (Table 4; Appendix 2). The sand geochemistry for each provenance type is in agreement with the composition of their inferred source areas. For example, the Snoqualmie batholith contains intermediate to felsic calc-alkaline arc rocks that were derived from an enriched mafic mantle source that underwent assimilation and fractional crystallization (Dragovich and others, 2009b,c). This agrees well with the geochemistry of units Qa, Qc_o , Qc_{ws} , and Qc_{pf} (Fig. 1a and 1b; Appendix 4, Fig. 1, 2, 3, and 4), which are ancient Snoqualmie River alluvium derived partially from erosion the Snoqualmie batholith (Table 4).

Figure 1D displays the chondrite-normalized La/Lu versus the chondrite-normalized Pb/Yb ratios for the average values from each Quaternary sedimentary unit. Even though many units are only represented by few data, some important observations on provenance can be derived from inspection of this figure in concert with examination of petrography and general provenance of the sands (Table 4 and Appendix 2). The average values for glacial deposits Qgod, Qga, Qgo, and Qgd all have lower chondrite-normalized La/Lu and Pb/Yb ratios than nonglacially derived units (Fig. 1D). This is attributed to the higher abundance of northerly derived lithic clasts within these samples (Table 4). Glacial units Qgos and Qgik plot closer to nonglacially derived averages; this is due primarily to excavation of older nonglacial units by recessional meltwater near and underlying these deposits (Appendix 2). The average value for nonglacial unit Qc_{wp} has a lower chondrite-normalized Pb/Yb ratio than ratios for other nonglacial units, which is in agreement with its derivation from a more andesitic Puget Group provenance (Table 4) than other nonglacial units (Fig. 1D). The nonglacial units Qa (Tolt River) and Qc_{ol} plot within very close proximity to each other on the chondrite-normalized La/Lu and Pb/Yb diagram (Fig. 1D). This supports their local eastern provenance (see petrography in Appendix 2 and Table 4), and helps distinguish these sands from Snoqualmie provenance sand samples (Fig. 1D). Unit Qc_{ol} in the eastern part of the Carnation quadrangle probably had a depositional environment very similar to the modern Tolt River, which is supported by the geochemical similarity between these samples. Average values for Snoqualmie provenance units Qc_o and Qc_{ws} have chondrite-normalized La/Lu and Pb/Yb ratios that are very similar, suggesting that their ancient Snoqualmie River alluvial source area is comparable (Fig. 1D; Table 4). The average values for Snoqualmie provenance units Qc_{pf} and Qa have higher chondrite-normalized La/Lu and Pb/Yb ratios,

suggesting that their source area may have been richer in felsic plutonic material (Fig. 1D). Overall, all of the SP units in Table 4 have similar chondrite-normalized La/Lu versus the chondrite normalized Pb/Yb ratios consistent with the sand grain petrography presented in Appendix 2.

Igneous Rock Geochemistry of the Volcanic Rocks of Mount Persis

Although the sample size is small, some general findings can be made for the volcanic rocks of Mount Persis of Tabor and others (1993). These samples are predominantly calc-alkaline (Appendix 4, Fig. 5 and 6), have elevated Th/Yb ratios (Appendix 4, Fig. 6), plot within or near the fields defined by continental arcs (Appendix 4, Fig. 6 and 7), and are predominantly peraluminous (Appendix 2). This is commonly found in “Corderillan” continental arcs (Pearce, 1983; Frost and others, 2001). Results here that show two samples possibly being transitional to tholeiitic and one sample being metaluminous are still consistent with this setting. The higher $\text{Na}_2\text{O}+\text{K}_2\text{O}$ and SiO_2 (Fig. 1C) and similar Ta/Yb ratios (Appendix 4, Fig. 6) indicate that the vitric tuffs fractionated from the other Mount Persis rocks. The low to moderate K_2O (Appendix 4, Fig. 5), elevated Ta/Yb ratios (Appendix 4, Fig. 6), and La/Yb ratios (Appendix 4, Fig. 7) suggest that these rocks originated from an enriched mafic source that may have undergone very minor amounts of assimilation (Bailey, 1981; Pearce, 1982, 1983).

Andesite flows and rhyolite tuffs (unit Eva_p) — Two flows from the volcanic rocks of Mount Persis (Tabor and others, 1993), one sample from this study (15M) and the other (76H) from Dragovich and others (2009c), both plot within the andesite field on the total alkali-silica (TAS) diagram (Fig. 1C). Two vitric tuffs from Mount Persis, both from Dragovich and others (2009c), plot within the rhyolite field on the TAS diagram (Fig. 1C). These two flows have an aluminum saturation index (ASI) that ranges from 1.01 to 1.03 and are peraluminous (Appendix 2). The vitric tuffs have ASIs that range from 1.17 to 1.41 and are peraluminous (Dragovich and others, 2009c). One flow (sample 76H) plots along the boundary between tholeiitic and medium-K calc-alkaline fields on the $\text{K}_2\text{O}-\text{SiO}_2$ diagram; while the other flow (15M) plots within the medium-K calc-alkaline field (Appendix 4, Fig. 5). Both vitric tuffs plot within the medium-K calc-alkaline fields on the $\text{K}_2\text{O}-\text{SiO}_2$ diagram (Appendix 4, Fig. 5). On the Th/Yb-Ta/Yb tectonic discrimination diagram of Pearce (1982, 1983), unit Eva_p volcanic flow samples plot within the calc-alkaline and continental arcs fields (Appendix 4, Fig. 6). Their Ta/Yb ratios suggest that these samples are originating from an enriched mantle source (Pearce, 1982, 1983) (Appendix 4, Fig. 5). On the La/Yb-Sc/Ni andesite discrimination diagram of Bailey (1981), flow 15M plots within the field for continental arcs, while flow 76H has a higher La/Yb ratio and plots between the continental arc and Andean arc fields (Appendix 4, Fig. 7). The vitric tuffs plot near the field defined by the Andean arc (Appendix 4, Fig. 7).

Volcanic breccia (unit Evb_p) — A pyroclastic breccia plots within the dacite field on the TAS diagram (Fig. 1c). This breccia has an ASI of 0.94 and is slightly metaluminous (Appendix 2). It plots within the tholeiitic field on the $\text{K}_2\text{O}-\text{SiO}_2$ diagram (Appendix 4, Fig. 5). On the Th/Yb-Ta/Yb tectonic discrimination diagram of Pearce (1982, 1983), the pyroclastic breccia plots within the calc-alkaline and continental arcs fields, but near the shoshonitic boundary (Appendix 4, Fig. 6). Its Ta/Yb ratios suggest that this breccia originating from an enriched mantle source (Pearce, 1982, 1983) (Appendix 4, Fig. 5). On the La/Yb-Sc/Ni andesite discrimination diagram of Bailey (1981), the pyroclastic breccia plots between the continental arc and Andean arc fields (Appendix 4, Fig. 7).

Lahars (unit Evl_p) — One clast from a semi-cohesive thick lahar bed plots within the andesite field on the TAS diagram (Fig. 1c). The ASI of this clast is 2.37 and it is peraluminous; however, this sample's chemical index of alteration (CIA) is moderately high (0.67) and the very high ASI could be a result of Al concentration during alteration (Appendix 2). This clast plots within the medium-K calc-alkaline field on the $\text{K}_2\text{O}-\text{SiO}_2$ diagram (Appendix 4, Fig. 5). On the Th/Yb-Ta/Yb tectonic discrimination diagram of Pearce (1982, 1983), this clast plots within the calc-alkaline and continental arcs fields (Appendix 4, Fig. 6). Its Ta/Yb ratios suggest that this breccia originated from a moderately enriched mantle source (Pearce, 1982, 1983) (Appendix 4, Fig. 5). On the La/Yb-Sc/Ni andesite discrimination diagram of Bailey (1981) this clast plots within the continental arc field (Appendix 4, Fig. 7). The high chemical index of alteration is consistent with petrographic observations of the lahar clasts which suggest the lahars were derived from an altered volcanic parent material. Perhaps the lahars were derived from the collapse of a highly altered Eocene edifice east of the map area (Dragovich and others, 2010).

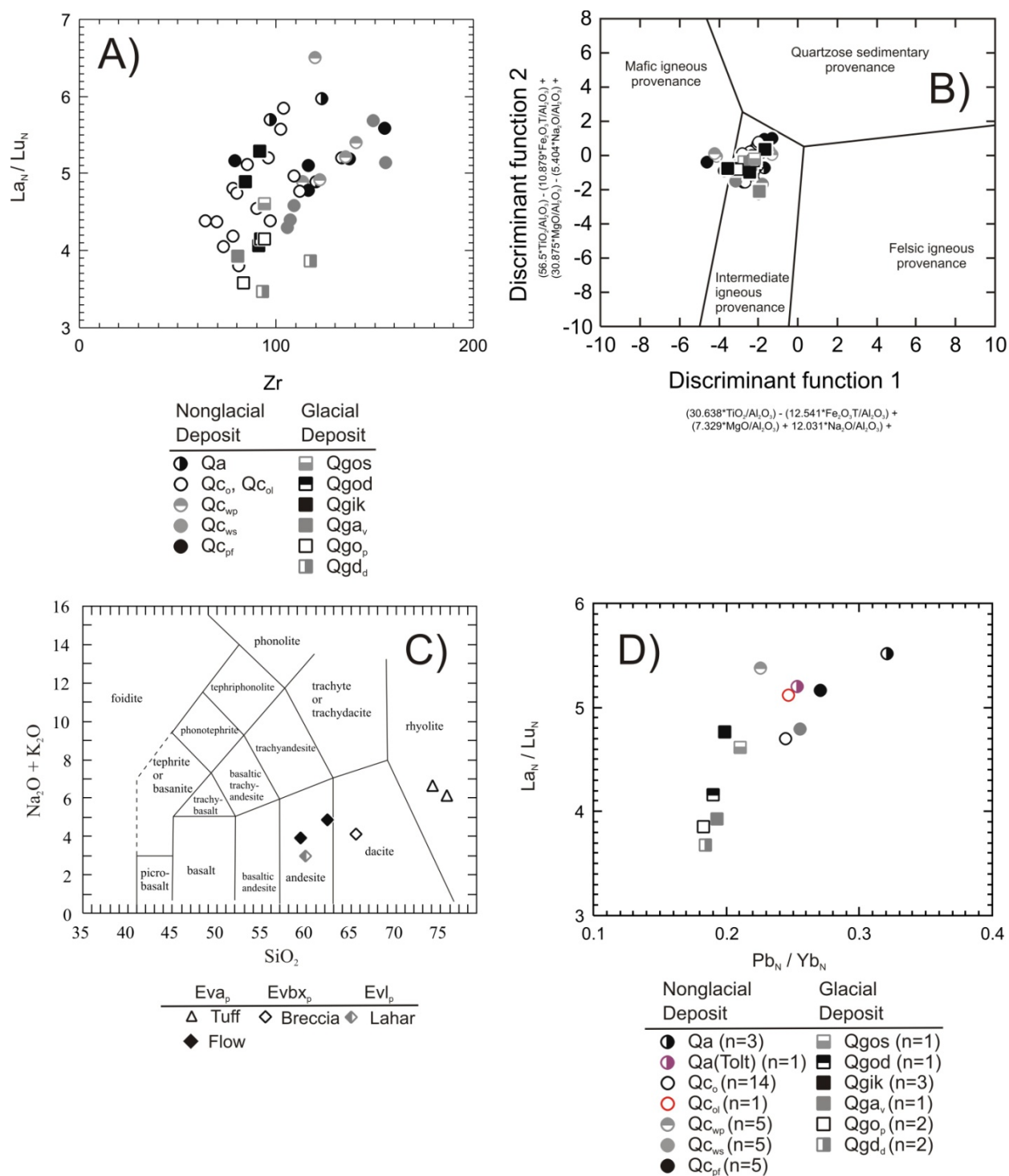


Figure 1: Sands from the Carnation 7.5-minute quadrangle plotted on: A) Chondrite normalized La/Lu vs. Zr (ppm) diagram. Normalization values from McDonough and Sun (1995); and B) Discriminant function diagram for the provenance of sedimentary rocks (after Roser and Korsch, 1988). Symbols the same as 1A; C) Volcanic rocks of the Mount Persis (Tabor and others, 1993) plotted on the total-alkalis vs. silica diagram of Le Maitre and others (2002); D) Chondrite normalized La/Lu versus Pb/Yb diagram for the average value of glacially and nonglacially derived sands from the Carnation 7.5-minute quadrangle. Note that the symbols are slightly different than other figures. Normalization values from McDonough and Sun (1995).

ISOSTATIC GRAVITY AND AEROMAGNETIC DATA FOR THE CARNATION QUADRANGLE

Methods

GEOPHYSICAL MAP

Aeromagnetic data come from a survey contracted by the U.S. Geological Survey in 1997. Flight lines are oriented north–south and have a 250-m spacing (Blakely and others, 1999). Magnetic anomalies for the map area are strongly asymmetric with respect to their source, therefore, we present a reduced-to-pole aeromagnetic anomaly map, calculated using standard procedures (Blakely, 1995). This filter moves magnetic anomalies directly over the magnetic source units (Figure 2A). For interpretation purposes, we upward continue the reduced-to-pole magnetic grid to 50 m above the flight altitude and then subtract the product from our original magnetic grid. The result is a map that isolates the anomalies produced by near-surface magnetic rocks. Recent data constrain the gravity anomalies for this region (Anderson and others, 2006; Dragovich and others, 2007, 2009a,b). Standard formulas and reduction procedures (Blakely, 1995), as well as a reduction density of 2670 kg/m³ for the crust, constrain the isostatic gravity anomaly contours.

GEOPHYSICAL MODELING

Geophysical cross section models were calculated with GM-SYS Geophysical Modeling software (NGA, Inc.). Sampling of the magnetic grid for the model profile is 250 m, similar to the spacing of flight lines on the aeromagnetic survey. Magnetic measurement altitudes in the profile are matched to the airplane altitude recorded by radar altimeter during the aeromagnetic survey. Gravity constraint is considerably sparser, more on the order of a grid with spacing of 1 km between stations (Figure 2A). We only display gravity data points on the profiles that lie within 1.5 km of the map profile line. Therefore, some of the details that are less than 1 km in width on the profile that are based on geologic mapping, though matching the existing gravity grid, are not well constrained.

ROCK PHYSICAL PROPERTIES

Density and magnetic properties of the rock units used in the map interpretation and two-dimensional geophysical modeling are supported by hand sample and outcrop magnetic susceptibility measurements, as well as hand sample density measurements (Anderson and others, 2006; Megan Anderson, unpub. data, 2006–2010). Where density and magnetic susceptibility measurements are not available, we apply reasonable densities from past geophysical modeling in the region (Dragovich and others, 2007; 2009a,b). Geophysical properties of “combined” units are averaged from hand samples of each component, based on the percentage of each component exposed in outcrops in the area. For example, the volcanic rocks of Mount Persis of Tabor and others (1993) contains more magnetic units (andesite flows) in the eastern part of the quadrangle than the west (Dragovich and others, 2010); the volcanic center for the volcanic rocks of Mount Persis is east of the Carnation quadrangle, thus fewer flows and more volcanoclastic rocks occur to the west (see unit Evs_p of Dragovich and others [2010]). Our modeling procedure honors both the mapped lithologic boundaries and the thickness of Quaternary sediments across the profiles. For example, see the bedrock top contour map in Appendix 5 and Cross Sections A and B of Dragovich and others (2010). Deeper boundaries are based solely on the geophysical evidence and structural inference. Basement properties are partially based on modeling from areas farther to the west in the Puget Lowland (Anderson and others, 2006) with small adjustments to densities/magnetic susceptibilities that allows better data fit for geophysical models in this region.

Interpretation

GEOPHYSICAL MAP

The most magnetic unit of the quadrangle is the andesite flows of the volcanic rocks of Mount Persis supported by our own hand sample measurements as well as other studies (e.g. Sherrod and others, 2008). This is reflected by the relatively high magnetic anomaly filling the northeastern corner of the aeromagnetic map (MPAF in Figure 2A). Based on the spatial limitation of the flows along ancient river valleys and drainages, it is likely that magnetic rocks contributing to this unit were sourced to the east or northeast of the quadrangle area. Slight variations in the intensity of the aeromagnetic anomaly may result from slight thickness changes in the unit across the region as well as variations in the magnetism of the unit.

Isostatic gravity anomalies largely reflect the Seattle basin deepening westward, thus the overall gradient with decreasing anomaly values to the west (Figure 2A). This overall decrease in values is superimposed by shorter wavelength and smaller amplitude gradients. We interpret faults to generally follow these local gravity gradients as well as a few magnetic gradients (for individual fault summaries see Appendix 8). Locations of gradients are mathematically determined through a maximum gradient computation for both the isostatic gravity and reduced-to-pole (RTP) aeromagnetic anomaly data. Both strands of the Carnation fault, in particular, are represented by a prominent gradient in the magnetic data (CFG; Figure 2A). The fault appears to have a reverse fault sense, bringing magnetic rocks closer to the surface to the north of the gradient. The gradient in the RTP anomaly map matches the position of a gradient in the near-surface magnetic grid, which indicates a relatively steeply-dipping structure such as reverse fault. The gradient is strongest in the original RTP data, therefore, though we modeled the magnetic anomalies in the cross sections with changes in depth and magnetization of the volcanic rocks of Mount Persis, there could be some associated offset of magnetic units in the deeper Western mélange belt, which we model with relatively uniform densities and susceptibilities in this region, but is locally variable in other nearby regions (Dragovich and others, 2009a,b,c). The strength of this gradient requires both a drop in magnetization and increase in depth of the volcanic rocks of Mount Persis south of the Carnation fault. This is consistent with the general interpretation of high-magnetization andesite flow-dominated packages within the unit as more proximal volcanic flows and conversely, low-magnetization clastic packages as more distal, volcanic sediments. This is a trend observed in other parts of the region (Dragovich and others, 2007, 2009b,c) and matches a few hand sample susceptibility measurements that show generally lower magnetic susceptibility for more volcanoclastic rocks such as volcanic sandstones or tuffaceous siltstones. Therefore, while faults in the region allow for an increase in depth of units to the west, these western Persis units are also more distant from volcanic source(s) and therefore contain more fluvial sediment and fewer andesite flows.

GEOPHYSICAL CROSS SECTION MODELS

Due to the complexity of the subsurface geology, there are many possible subsurface rock geometries that will fit our geophysical data. Cross Sections A-A' and B-B' (Figure 2B-2C) were modified from original structural inference to fit the observed gravity and magnetic data. Increase in sediment density with depth broadly follows Anderson and others (2006). The position of fault-bounded rock packages matches well with the initial determinations derived solely from structural-stratigraphic inferences in the geologic cross section models in Dragovich and others (2010). The contrast in physical properties across the boundary in the basement (along RMF #1 in A-A' and B-B'; Figures 2B-2C) is more subtle here than in quadrangles to the south of the present map area (Dragovich and others, 2007, 2009a,b,c), but making a distinction helps with a better fit of the geophysical data. Distinctions between different types of "Seattle basin fill" (volcanic rocks of Snoqualmie Falls, Blakely Formation, Puget Group, volcanic rocks of Mount Persis) are not distinguishable by the gravity data. What is generally reflected in the gravity anomaly data is the increase in sediment depth to the west and the large jump in sediment thickness at the main strand of the Rattlesnake Mountain fault zone (RMF #1 in Figures 2B-2C), which is supported by an increase in gravity gradient across this fundamental structure. Sediment thickness can trade off with densities of these units, especially for the Puget Group, therefore the exact basin depth is not well-constrained because of uncertainty in sediment density. Low-density cataclasite (unit tz) along faults is not as critical for modeling the gravity data here as for quadrangles further south such as the North Bend quadrangle (Dragovich and others, 2009a) and could trade off with density of overlying sedimentary units. They are included based

on: (1) observations of cataclasite or deformed Quaternary deposits (unit Qtz) within the map area; (2) observation of broad zones of unit tz along some of these faults in quadrangles south of the map area (Dragovich and others, 2007, 2009a,b,c) and (3) our contention that some of the faults (such as RMF-1 and SVF-1) are major and long-lived tectonic boundaries that have accumulated much permanent strain. Including a low density tz unit particularly helps to fit the low gravity associated with RMF #1 and #5 and unnamed faults (model A-A'; Figure 2B). However, we qualify this interpretation with the observation that variation of density within Seattle basin-filling lithologies could also cause such variations in the gravity.

The volcanic rocks of Mount Persis (Mt. Persis unit) decrease in magnetic susceptibility from northeast to southwest, which is largely responsible for overall declining gradient in the model cross sections, particularly along A-A' (Figure 2B). A magnetic Mt. Persis unit is also used in modeling of geophysical data in Sherrod and others (2008), and the aeromagnetic high in this quadrangle is contiguous with their anomaly B. We use only a slightly higher susceptibility for the Mt. Persis unit in our models ($\chi = 30 \times 10^{-3}$ SI maximum in our region as opposed to $\chi \sim 24 \times 10^{-3}$ SI for Sherrod and others, 2008), but include the magnetic units as flows within a shallower (with the top at 100-400 m) and thinner (275 m) Mount Persis unit, contrasting the model of Sherrod and others (2008) who put the top at 0-4 km and use a thickness of 1-3 km. Our thickness for the volcanic rocks of Mount Persis is based on regional considerations of boring data (Rau and Johnson, 1999), structural inference (Dragovich and others, 2010), as well as measured section by Danner (1957) north of the Carnation quadrangle; similarly, other units in the model are constrained by similar geologic data (Capps and others, 1973; Yount and Gower, 1991; Lindquist, 1957). Because of the likelihood that the volcanic rocks of Mt. Persis is not a regional unit, but has a distribution more consistent with isolated volcanic center(s) east of the Carnation quadrangle, we prefer the interpretation that the Persis unit interfingers with the uppermost part of the Puget Group and is limited in distribution and thickness, particularly west of Rattlesnake Mountain fault no. 1 (Figures 2B and C). Though we handle the modeling of this unit differently than Sherrod and others (2008), our overall tectonic conclusions are the same: our data and modeling support steeply dipping faults and oblique-right-slip faulting in the region. Given that the Whidbey Island Fault zone modeled by Sherrod and others (2008) and the zone of faults in this quadrangle likely connect, this similar conclusion is encouraging.

The volcanic unit in the Blakeley Formation (modeled in A-A'; Figure 2B) is evidenced within the aeromagnetic anomaly map data on the edge of and west of the quadrangle area (BV in Figure 2A) and is necessary to fit the aeromagnetic anomaly data in model A-A' (Figure 2B). The inclusion of the magnetic volcanic body in the Blakeley is supported by our observation that the Blakeley Formation contains volcanic beds locally. An alternative hypothesis is that the magnetic anomaly BV may actually be emanating from Miocene volcanic rocks overlying the Blakeley Formation along the western portion of the map area. The anomaly might be sourced by Miocene volcanic rocks such as the pyroclastic deposits correlated with the volcanic rocks of Snoqualmie Falls directly northwest of the Carnation quadrangle and dated during this study (Appendix 6). This hypothesis is allowable, given the trade-offs between strength of magnetism of the rocks and their depth—therefore the unit could be shallower and less magnetic, yet produce a similar magnetic anomaly. Further work is required to identify the source of the magnetic anomaly along the western portion of the map area. Regardless of the source unit, this volcanic layer must end at the “unnamed” faults for a good fit of the model to the aeromagnetic data. This supports these unnamed faults as well as RMF #5 as part of a major basin bounding system including RMF #1. Fitting the magnetic anomaly data requires the volcanic body to be truncated just west of the unnamed faults, thus supports the inclusion of a wide zone of tz within the RMF zone. We speculate that the anomaly might be due to Miocene pyroclastic deposits and other relatively magnetically susceptible volcanic and volcanoclastic rocks preserved in a basin that were offset along the main strand of the Rattlesnake Mountain fault zone from their original source to the southeast of the map area.

Figure 2A: Geophysical map of the Carnation quadrangle (*following page*). Base map is the reduced-to-pole aeromagnetic anomaly map with isostatic gravity contours (1 mGal interval) superimposed, labeled in mGals. Darker lines are interpreted faults from Dragovich and others (2010). See Dragovich and others (2010) and Appendix 8 for additional information on individual faults. Cross sections A-A' and B-B' coincide with cross sections in Dragovich and others (2010) and are shown in Figures 2B and 2C, respectively. Crosses indicate locations of gravity measurements controlling the isostatic gravity grid. BV, Blakely Formation volcanic unit (low amplitude magnetic high), CFG, Carnation fault gradient, MPAF, Mount Persis andesite flows (magnetic high). Fault names: CCFZ, Cherry Creek fault zone; CVF, Cherry Valley fault; CF#1, Carnation fault no. 1; CF#2, Carnation fault no. 2; SVF#1, Snoqualmie Valley fault no. 1; SVF#2, Snoqualmie Valley fault no. 2; SVF#3, Snoqualmie Valley fault no. 3; RMF#1, Rattlesnake Mountain fault no. 1; RMF#5, Rattlesnake Mountain fault no. 5;

Figure 2B: Geophysical model along cross section A-A' presented *two pages below*. Cross section location shown in Figure 2A. Key to unit colors is given in Figure 2D presented four pages below; percentage of andesitic flows depicted in the volcanic rocks of Mt. Persis is directly related to relative changes in magnetism of this unit across the profile; volume of interbedded Mt. Persis flows are inferred to decrease to the west. The model is assumed to extend to infinity in both directions perpendicular to the profile. The blue triangles in the lower panel indicate the height of the flight line above the ground for the aeromagnetic data. Vertical exaggeration is 3X for both geophysical cross sections. Solid lines show fault locations that are controlled by the geophysical data. Dashed lines show fault locations that are controlled by geologic mapping at the surface, but are less certain at depth. Most faults are transpressive. RMF, Rattlesnake Mountain fault; SVF, Snoqualmie Valley fault; CHCF, Cherry Creek fault; CHVF Cherry Creek fault zone; CF, Carnation fault.

Figure 2C: Geophysical model along cross section B-B' presented *three pages below*. Cross section location shown in Figure 2A. See Figure 2B caption (above) for more information.

Figure 2A. See caption on preceding page.

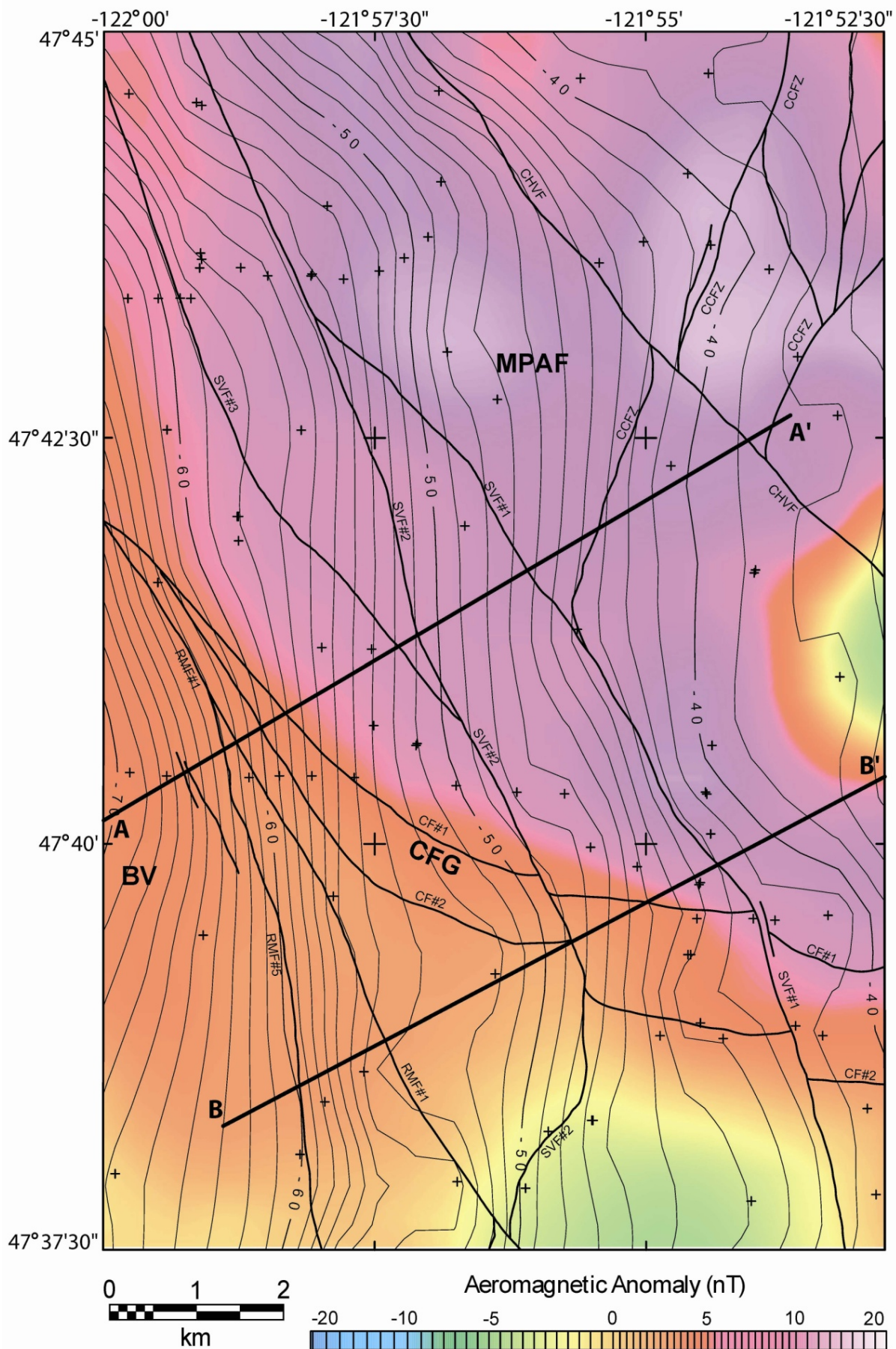


Figure 2B. Caption on page preceding Figure 2A.

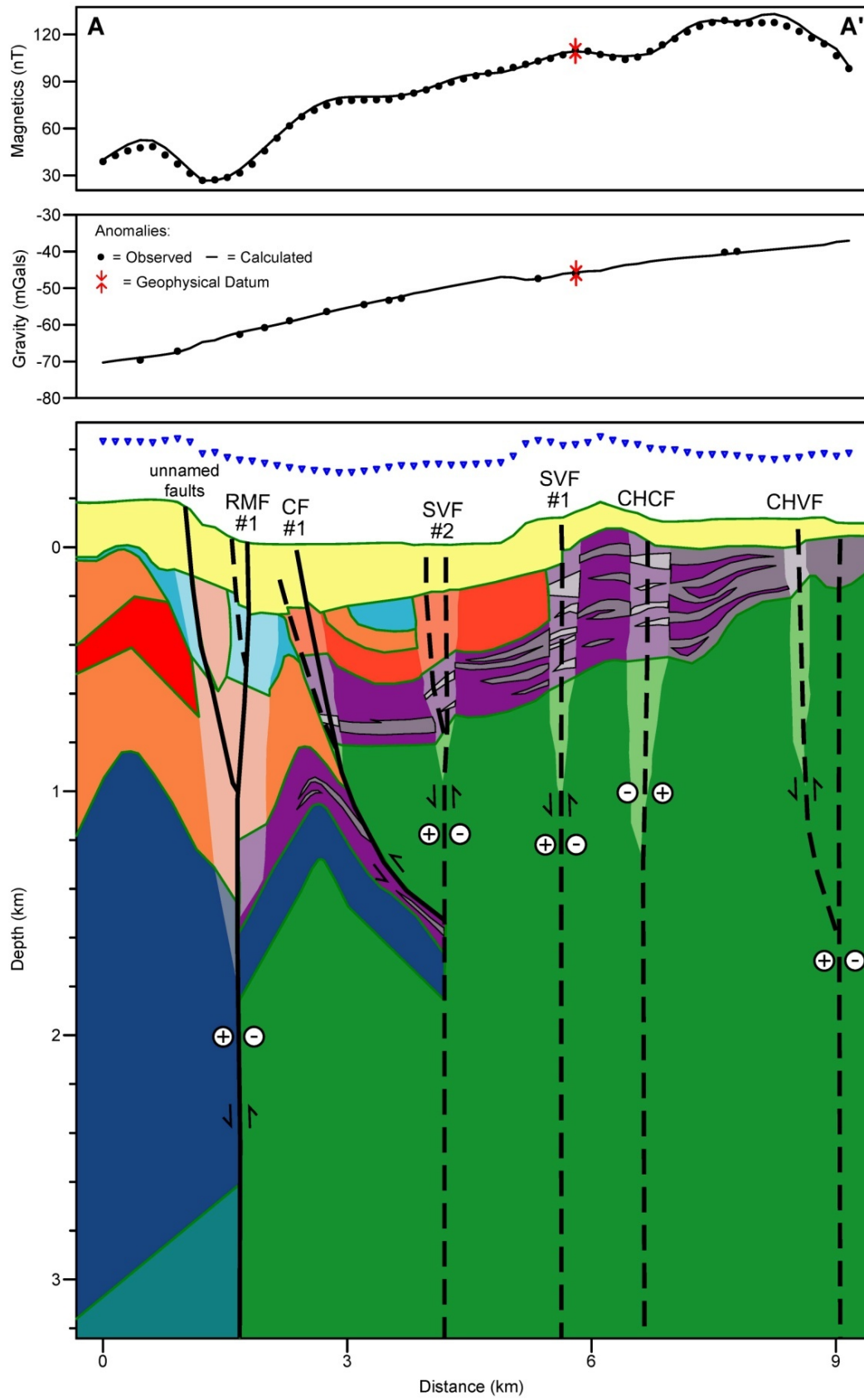
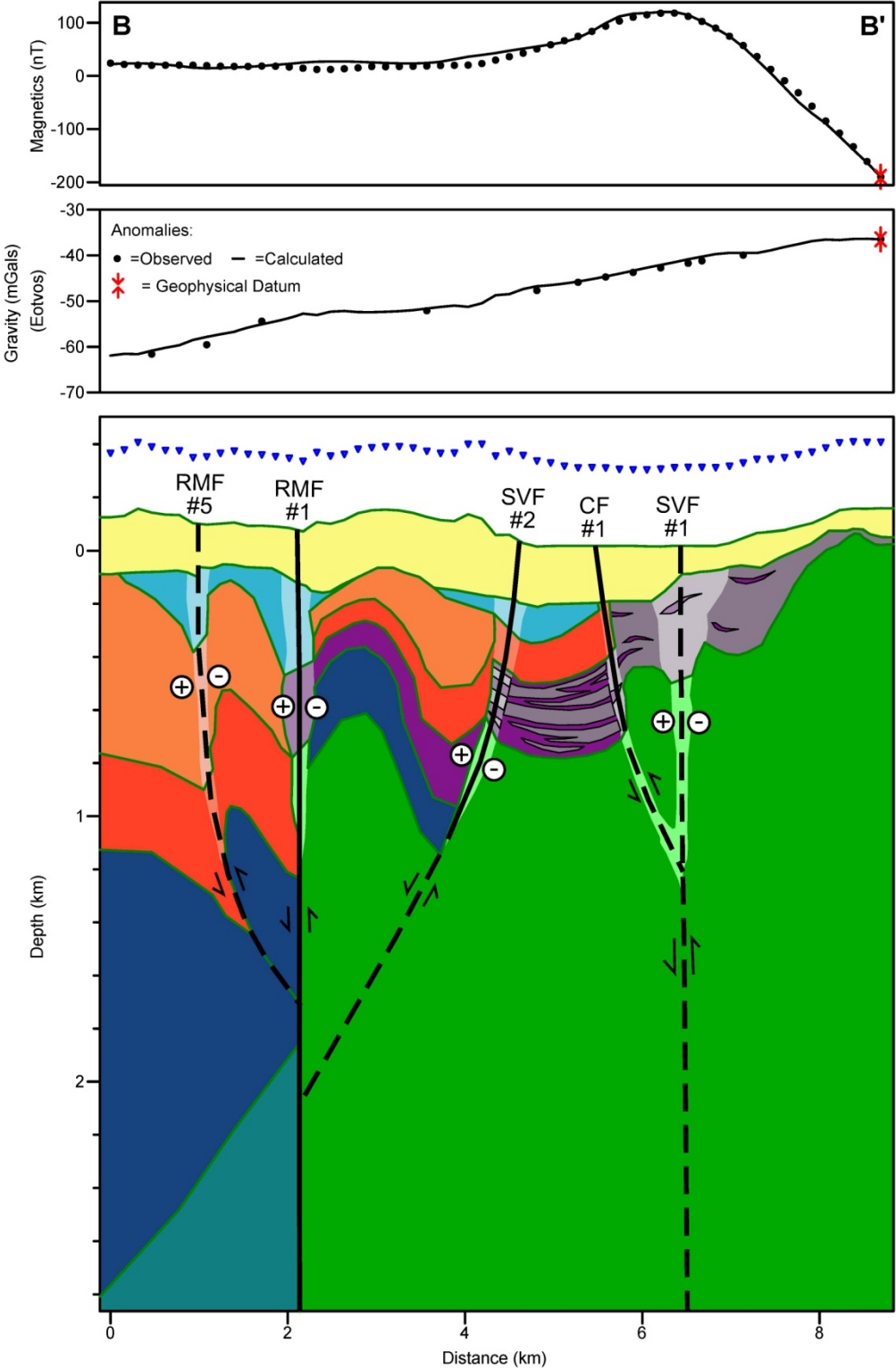


Figure 2C. Caption on page preceding Figure 2A.




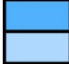

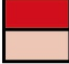

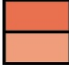
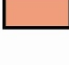

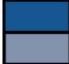




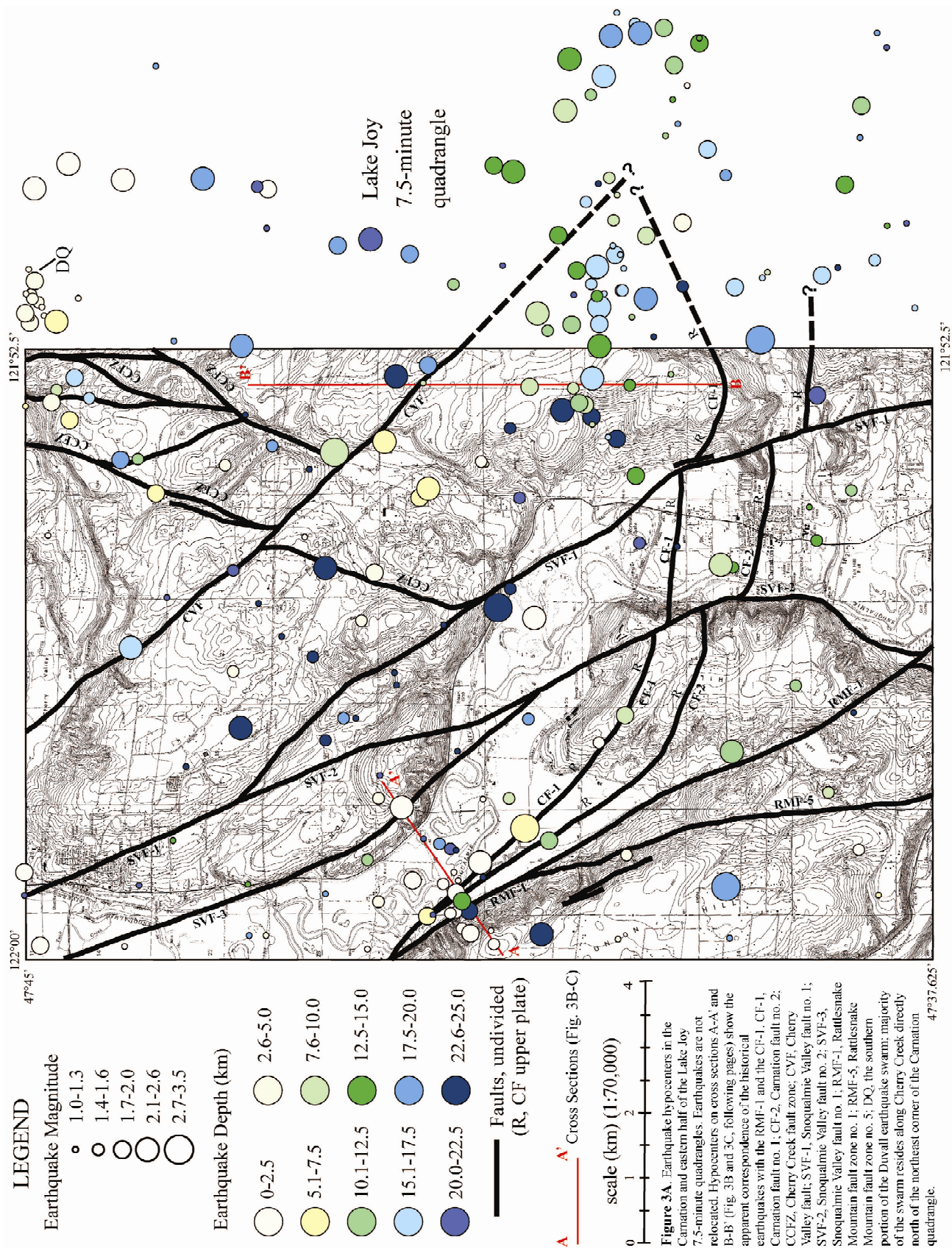
	$\Delta\rho = -620$ $\chi = 2.7$	Quaternary sediments (all Quaternary geologic units)
	$\Delta\rho = -430$ $\chi = 0$ $\Delta\rho = -470$	Miocene sedimentary and volcanic rocks undifferentiated (unit Mvc) cataclasite of unit Mvc (unit tz)
	$\Delta\rho = -520$ $\chi = 0$	Blakeley Formation (nearshore and marine)(unit OEn)
	$\Delta\rho = -520$ $\chi = 13$	Blakeley Formation (volcanic rocks undifferentiated)(see text)
	$\Delta\rho = -520$ $\chi = 0$	cataclasite of Blakeley Formation (unit tz)
	$\Delta\rho = -430$ $\chi = 0$	rocks of Bulson Creek and (or) Blakely Formation nonmarine (fluvial) units (unit OEc)
	$\Delta\rho = -470$	cataclasite of OEc (unit tz)
	$\Delta\rho = -284$ $\chi = 16.4$ $\Delta\rho = -328$	volcanic rocks of Mt. Persis; light purple, Eva(p) flows; dark purple, unit Evs(p) volcanics cataclasite of volcanic rocks of Mt. Persis (unit tz)
	$\Delta\rho = -170$ $\chi = 0$	Puget Group undifferentiated (unit Evs(pg))
	$\Delta\rho = -270$	cataclasite of unit Evs(pg) (unit tz)
	$\Delta\rho = -10$ $\chi = 3-5$	Western melange belt undifferentiated (unit KJm)
	$\Delta\rho = -10$	cataclasite of unit KJm (unit tz)
	$\Delta\rho = -10$ $\chi = 1$	undifferentiated basement

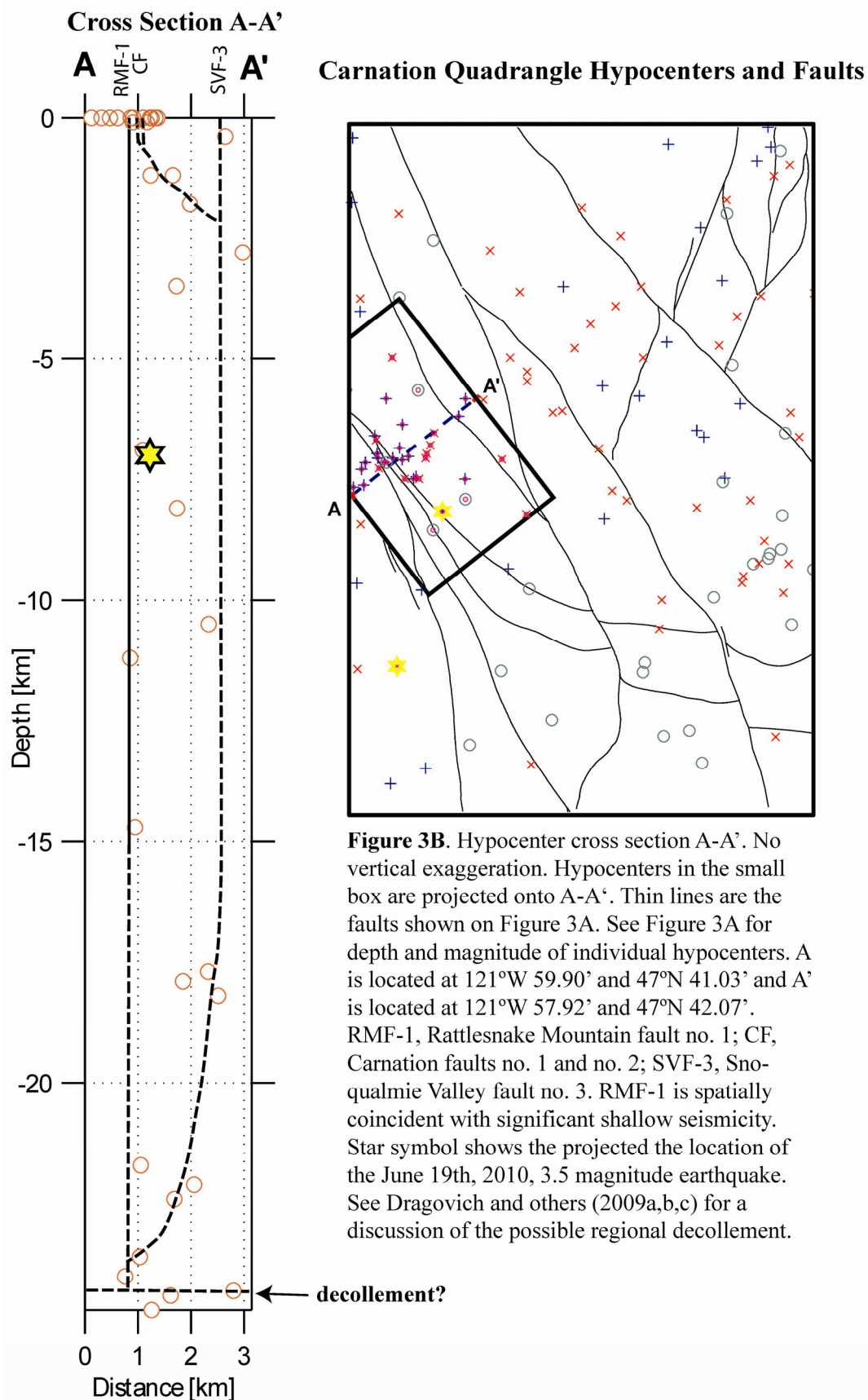
Figure 2D: Key to units in Figures 2B and 2C. $\Delta\rho$ is the density contrast relative to normal crust (2670) in kg/m^3 ; χ is magnetic susceptibility in SI units multiplied by 1000. Cataclasite units (shown as lighter colors) carry similar magnetic properties to equivalent geologic units that are not cataclastically deformed. Note the distinction between andesite flows (light purple) and volcanoclastic and tuffaceous rocks (dark purple) of the volcanic rocks of Mount Persis. See the corresponding geologic unit (for example, Mvc) in Dragovich and others (2010) for more lithologic and structural information on each of these modeled units. Undifferentiated basement is below cross sections A and B of Dragovich and others (2010) and only discussed in this document. See Dragovich and others (2009a,b) for a discussion of 'undifferentiated basement' in the Snoqualmie and North Bend area south of the Carnation quadrangle. Compare bedrock top elevation map provided in Appendix 5 with Quaternary sediment thicknesses shown here and in Dragovich and others (2010).

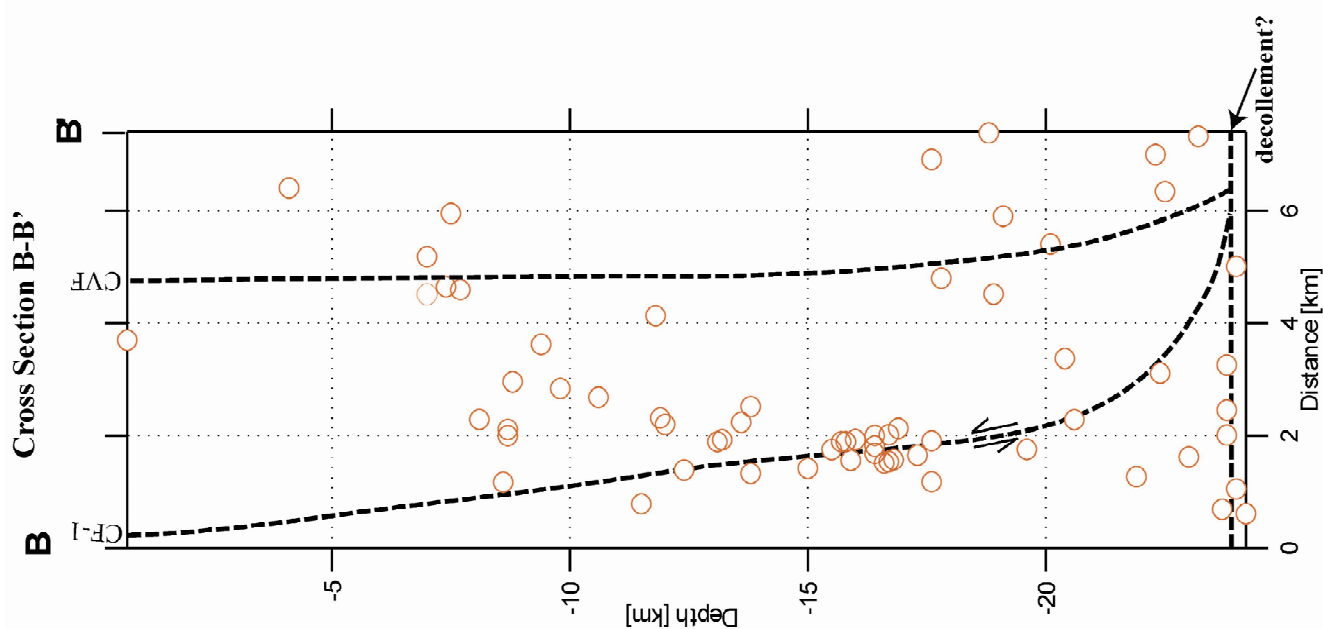
EARTHQUAKE HYPOCENTERS IN AND NEAR THE CARNATION QUADRANGLE

We obtained the hypocenters shown in Figure 3A-C from Pacific Northwest Seismic Network. The earthquake catalog data were downloaded from the Advanced National Seismic System (ANSS) web site (URL: <http://quake.geo.berkeley.edu/anss/catalog-search.html>). We analyzed the hypocenters, by using ZMAP—a tool for visualizing seismicity patterns (Wyss and others, 2001). The hypocenters for the western half of the Lake Joy 7.5-minute quadrangle are included in our analyses because we suspect some of that seismicity may be emanating from the Carnation fault. (See comments on earthquake hypocenters in Appendix 8).

The earthquake data are not relocated and are not filtered for quality and thus can only be used as a general guide for structural interpretation. The data suggests that: (1) Rattlesnake Mountain fault zone no. 1 is active (Figure 3B) and is coincident with significant shallow crustal seismicity; and (2) the Carnation fault may be active as indicated by the overall shallowing of the seismicity north of this moderately dipping fault (Figure 3C). The seismicity (from 1971 to 2010) covering most of the cataloged instrumental earthquake data suggests that Carnation fault no. 1 in the eastern part of the map area dips ~85 to the north in the upper part of the continental crust (Figure 3C).







Hypocenters and Faults Index Map

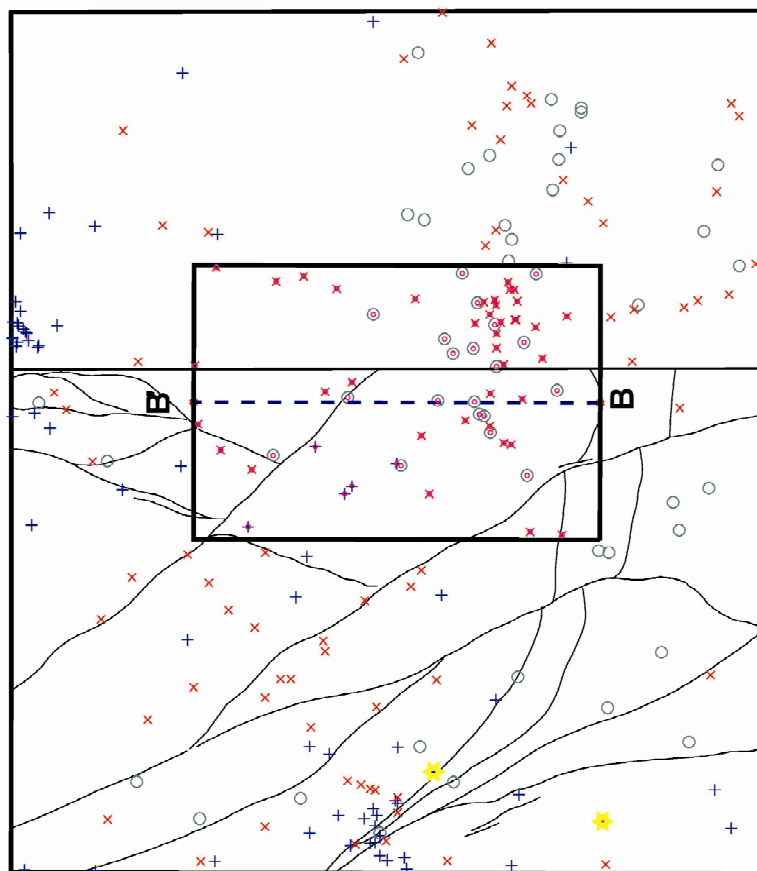


Figure 3C. Hypocenter cross section B-B'. No vertical exaggeration. Hypocenters in the small box are projected onto B-B'. Thin lines are the faults shown on Figure 3A. See Figure 3A for depth and magnitude of individual hypocenters. B is located at 121°W 53.04' and 47°N 39.22' and B' is located at 121°W 53.00' and 47°N 43. CF-1, Carnation fault no. 1; CVF, Cherry Valley fault. CF-1 may be spatially coincident with significant seismicity. See Dragovich and others (2009a,b,c) for a discussion of the possible regional decollement.

QUATERNARY DEFORMATION

Introduction

Obtaining direct field evidence for Holocene motion on fault strands in the region is complicated by the dense vegetative cover and urbanization. In lieu of trenching of suspected fault traces, fault investigations must rely on sparse outcroppings near topographic, geomorphic and geophysical lineaments or anomaly edges. Faults were mapped in the Carnation 7.5-minute quadrangle by Dragovich and others (2010) on the basis of our interpretation of geophysical anomalies (Figs. 2 and 3), geomorphologic lineaments, and stratigraphy, as well as our interpretation of deformational features observed in outcrop both locally and regionally (Dragovich and others, 2007, 2009a,b,c). Some faults are aligned with buried bedrock escarpments or lineaments, including buried ancient fluvial channels, which are illuminated by depth-to-bedrock mapping (Appendix 5). Photographs of some of the Quaternary deformational features observed in the map area are presented in Appendix 7. Findings relevant to each of the faults shown in the map area are summarized in Appendix 8 and discussed briefly below.

Neotectonic Features—Tectonic Deformation and Liquefaction

LIQUEFACTION FEATURES

Liquefaction features are widespread and locally very intense in the pre-Vashon nonglacial deposits of the map area (units Qc_o, Qc_{ws}, Qc_{pf}, Appendices 7 and 8) and some of the older glacial deposits (unit Qgd_a). Liquefaction features include sand dikes, diapirs, flames, destroyed or chaotic bedding, rootless tight to isoclinal folding, and rare dish structures (for example, see unit Qtz in Dragovich and others, 2010). In many areas, moderately intense to intense liquefaction was observed in successive exposures giving the impression that large volumes of strata had been liquefied. It is important to note that some small faults or fractures in liquefied beds might be ancient mass-wasting features related to lateral spreading. During earthquakes, liquefied bodies spread toward an open face such as a river terrace via lateral spreading, and some lateral-spread landslide scarps could have an appearance similar to tectonic faults. However, the overall impression along some of the mapped faults is one of intense liquefaction associated with fault tectonism and intrusion into dilating tectonic zones.

We suspect that some of this liquefaction is the result of strong and (or) prolonged shaking near some of the inferred faults and fault zones. Although liquefaction is not restricted to the nonglacial deposits, and has been noted locally in Vashon recessional and advance outwash and lake deposits and older glacial deposits, the intense and widespread occurrence of liquefaction in SP units (Table 4) infers that the ancient Snoqualmie River depositional environment was favorable for past liquefaction events. It is widely known that because alluvium is predominately saturated and loose, these granular deposits have a high potential for liquefaction. Given this potential, it begs the question: does the bulk of the liquefaction observed in ancient SP deposits record liquefaction concurrent with past deposition as flat-lying ancient Snoqualmie River deposits? We suspect the answer to this question is yes with a caveat for areas of intense liquefaction near faults. It could be argued that the widespread nature of this *low to moderate intensity liquefaction* in SP units (Table 4) seems best explained as spatially broad liquefaction resulting from earthquakes, perhaps regional earthquakes. However, the general volume of liquefied sediment relative to undisturbed sediment observed in other 7.5-minute quadrangles away from probable active faults suggests to us that much of the causative shaking must be local and related to nearby active faults. The long linear zones of *moderate to intense liquefaction* associated with some fault zones mapped using multi-disciplinary methods seem to be best explained as being the result of high ground accelerations along active faults zones; particularly along linear zones where intense liquefaction is supported by additional evidence for faulting, such as stratigraphic discontinuities, geophysical lineaments or earthquake hypocenters. This is particularly evident along: (1) Rattlesnake Mountain fault no. 1 (RMF-1) along the Snoqualmie Valley Road; (2) Snoqualmie Valley fault no. 2 (SVF-2) at the eastern foot of Tolt Hill, in MacDonald Park near the contact between Olympia beds and modern alluvium; (3) the northern part of the Cherry Valley fault; and (4) the southernmost part of Rattlesnake Mountain fault no. 5 (RMF-5).

We focus here on liquefaction features along southern part of SVF-2 because the outcrop-scale structures are best exposed along part of this fault zone. Along the eastern foot of Tolt Hill, Olympia beds contain sand and pebbly sand dikes and irregular bodies that intrude SVF-2. Many of the injectites are large volume bodies with diapir-like structure. These bodies have locally preserved bedding—bedding is mostly steeply dipping to vertical and commonly strikes E-W or ESE-WNE. This bedding is typically deformed into rootless folds that were attenuated during sediment fluidization accompanying liquefaction (photos in Appendix 7). Some of the apparent bedding may be flow banding. Several meter-thick zones of injectite containing rootless folds and extremely disrupted or destroyed bedding are bounded by areas with less intense liquefaction. We observed similar structures (intense and voluminous liquefaction-tectonic structures) in the Whidbey Formation and Double Bluff Drift along RMF-1 north of Ames Lake along the Snoqualmie Valley Road.

OVERVIEW OF QUATERNARY TECTONIC FEATURES IN THE SNOQUALMIE VALLEY

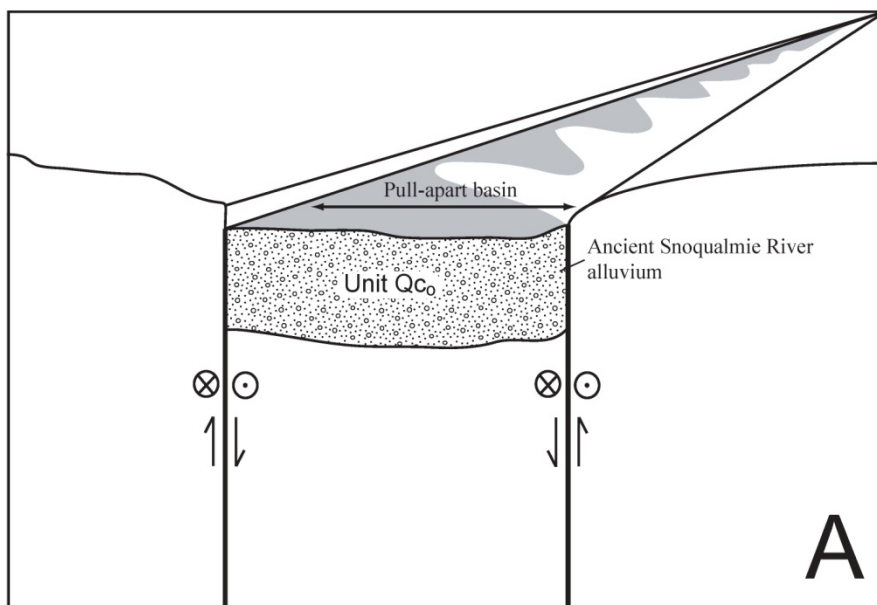
Structures that have been mapped in the Carnation quadrangle (this study) have been found to be extensions of, and correlative with, regional structures mapped by others elsewhere. For instance, the Rattlesnake Mountain fault zone (RMFZ) is a regional strike-slip fault zone that likely correlates with the Southern Whidbey Island fault (SWIF) of Dragovich and others (2009a,b,c and 2010) and Sherrod and others (2008). As such, it extends for miles to the northwest and a lesser distance to the southeast.

At the wider scale, structure in the Carnation quadrangle is dominated by a several wide fault zones that bound uplifted and down-dropped blocks showing evidence for both transtension and transpression. Individual fault strands throughout the area vary from strike-slip to oblique-slip faults. The northwest-trending Cherry Valley fault, which may correlate with the Griffin Creek fault of Dragovich and others (2009b,c), is interpreted to be the northeastern boundary of the RMFZ in the Carnation quadrangle. Broad Quaternary deformation and uplift is implied by the occurrence of tilted and broadly folded ancient Snoqualmie River alluvium (SP in Table 4) at (1) many stratigraphic levels, and (2) occupying elevated positions relative to the present position of the Snoqualmie River. Basin-wide deformational structures and uplift can also be inferred for SP units on the basis of (1) outcrop-scale tilting, folding, fracturing and faulting, and (2) anomalously high unit thickness. We conclude that the observed sedimentary structures and fault orientations are best explained as resulting from local transtension and transpression, creating growth folds, pull-apart and inverted basins within the broader zone of translation (Figure 4).

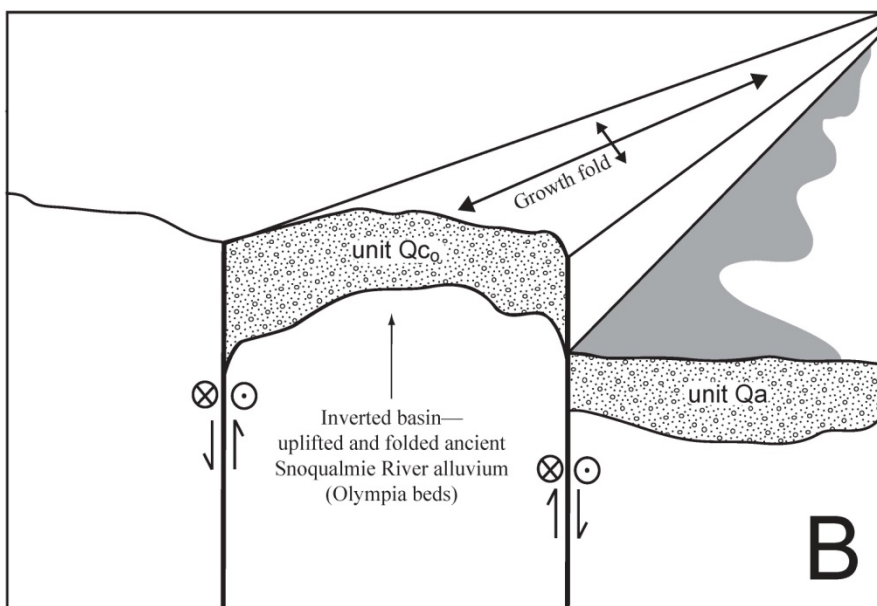
Dislocation on at least many of the mapped faults is thought to be long-lived, as evidenced by the presence of growth folds, which are the result of shortening during sedimentation. Because sedimentation accompanies shortening, growth folds exhibit subtle to distinct angular unconformities between major sequences of strata, and along the fold limbs, older strata dip more steeply. Stratigraphic relationships and structural style suggest strike-slip deformation concurrent with sedimentation since at least the early Miocene. This is probably best illustrated southeast of the present map area where the deposition and intrusion of Miocene volcanic rocks of Snoqualmie Falls are controlled by Rattlesnake Mountain fault zone (RMFZ) structural basins and basin-bounding faults including RMF-1 (Dragovich and others, 2009b). The Union Hill and Tolt Hill growth folds are inferred on the basis of stratigraphy, structural arrangements (for example, bedding orientations) and the bedrock-top elevations. We suspect that some of the other mapped folds in the study area are also growth folds (see Cross Sections A and B of Dragovich and others, 2010, and Tolt Hill growth fold in Dragovich and others, 2007).

Pull-apart basins are locally evident within the Rattlesnake Mountain Fault Zone at releasing bends and at some intersections with other structures. Some of the pull-apart basins were uplifted during later transpression to create inverted basins. Stratigraphy and sedimentary structures record both extension and later compression and uplift along the length of this complex fault zone (Dragovich and others, 2009a,b,c; Littke and others, 2009).

Figure 4. Basin inversion and uplift of ancient Snoqualmie River alluvium



Pull-apart structural control of ancient Snoqualmie River basins and deposition of ancient Snoqualmie River alluvium as the Olympia beds (unit Qc₀, 20–60 ka).



Growth-fold uplift and inversion of ancient alluvium within the Rattlesnake Mountain fault zone (for example, Snoqualmie Ridge). Unit Qa, Quaternary alluvium; unit Qc₀, ancient Snoqualmie River alluvium.

Petrology, geochemistry, geochronology, and sedimentary structures all indicate that the Pleistocene nonglacial deposits are mostly ancient Snoqualmie River alluvium (SP) that has been folded, faulted, tilted and uplifted between strands of the RMFZ (Table 4; Fig. 1A and 1D; Appendix 2, 4 and 6). Basin-wide deformational structures and uplift can be inferred for SP units on the basis of high local unit thickness, and elevated stratigraphic position in some areas where they may represent an inverted basin or basins. In this model for example, the majority of unit Qc, along Snoqualmie Ridge (>700 ft thick) in the Fall City and Snoqualmie 7.5-minute quadrangles was originally deposited in a RMFZ transtensional basin. Basin inversion was accomplished through uplift and folding during a later RMFZ transpressional phase (Dragovich and others, 2007, 2009b,c). In the Carnation quadrangle, the SP Olympia beds around Tolt Hill are thought to exhibit evidence of a growth fold. These beds are relatively thick and are presently elevated in the form of an inverted basin. The elevated stratigraphic position of thick SP units in some areas implies structural control over deposition. It is important to note that sea-level, thus base level, during the Olympia nonglacial interval was lower than present and so valley entrenchment would be expected, rather than elevated thick ancient SP alluvium.

The approximately 15 degree change in general azimuth of the SWIF trend along the western edge of the Carnation quadrangle from NNW to NW suggests an increase in transpressional deformation within the fault zone in the vicinity of Carnation. However, data constraining structural style and local stress regimes are not abundant, making statements like that above hypothetical. Given the paucity of mapped surface deformation and the limited utility of available subsurface data, other variations in structurally controlled deposition and uplift likely may only be confirmed using subsurface data in combination with geophysical modeling.

Individual Fault Features in the Carnation Quadrangle—Summaries and Activity

ACTIVITY

Quaternary tectonic deformational features observed in the map area include faults, fractures, and broad folding around growth folds. They are associated with liquefaction features, such as flames and sand dikes, as discussed above. Unit Qtz is mapped around areas of prominent Quaternary deformation along and near faults by Dragovich and others (2010). These areas are interpreted to be of neotectonic origin on the basis of deformational style and common association with liquefaction features. Some of the best-exposed areas of intense liquefaction and (or) probable tectonic deformation are located at (but not limited to) critical sites 14E, 14H, 24N, 25A, 25C, 43H, 45L, 45P, 53B, 66H, 81Z on Plate 1 of Dragovich and others (2010).

Some of the mapped faults are considered probable active faults but definitive evidence of Holocene activity awaits further study (for example, detailed fault trenching). *Active faults* as described here are considered to have evidence for offset during the Holocene (last ~11,000 yrs). The best evidence for active faulting includes displaced Holocene deposits combined with other evidence for on-going displacement such as well-located hypocenters along well-defined faults. *Potentially active faults* as described here have evidence for offset during Quaternary time which has been recently expanded to include the last ~2.6 million years. There is good evidence that several of the mapped faults in the study area are *potentially active* faults with some local evidence for *active* faulting along some of these structures. Probable tectonic deformation is recognized in all the ancient Snoqualmie River alluvial units (Table 4) including the Olympia Beds and the Whidbey Formation. It is also locally observed in Vashon recessional deposits (unit Qgos) as well as Vashon advance outwash and advance lake deposits (units Qgl_v and Qga_v) indicating that some of the deformation is likely Holocene. For example, probable tectonic faults displace recessional sand deposits along RMF-1 north of Ames Lake as illustrated in Figure 4 of Dragovich and others (2007). Complete characterization of these mapped faults awaits detailed analyses including fault trenching for both the proposed active faults and potentially active faults.

FAULT SUMMARIES

Here we document some of the attributes for the major faults mapped by Dragovich and others (2010). Several of these faults were originally mapped south and southeast of the Carnation quadrangle (Dragovich and others, 2007, 2009a,b,c) and extended into this area. Findings relevant to each of the faults are also summarized in a matrix format (Appendix 8). This table provides information concerning: (1) general fault characteristics; (2) gravity-magnetic mapping; (3) earthquake hypocenter information; (4) probable tectonic structures; (5) previous mapping or topical studies relevant to the fault inside and outside the quadrangle; (6) lidar or other geomorphic mapping; (7) age of tectonically deformed sediments; and (8) activity and overall certainty. We summarize or expand on some of this information below.

Rattlesnake Mountain fault no. 1 (RMF-1)—Probable to definite tectonic deformation of Quaternary deposits occur along this fault particularly in areas mapped as unit Qtz. The fault appears to displace recessional outwash near Ames Lake and is coincident with shallow hypocenters and thus appears to be active. This fault is geophysically prominent in the quadrangle. In the Snoqualmie quadrangle southeast of the map area, RMF-1 is coincident with a major subsurface boundary. Stratigraphic relationships across this fault near Snoqualmie Falls are indicative of a long-term fault that bounds the Snoqualmie basin where volcanic rocks of Snoqualmie Falls are juxtaposed against older volcanic rocks and the Puget Group (Dragovich and others, 2009b). The fault also bounds the Snoqualmie Valley basin in the westernmost part of the Snoqualmie quadrangle and the eastern part of the Fall City quadrangle (Dragovich and others, 2007, 2009b) and the southernmost part of the Carnation quadrangle. RMF-1 is likely correlative with the active Cottage Lake lineament of Sherrod and others (2008). One of several unresolved issues for this fault is why Holocene alluvial fans apparently are not offset across the trace of the fault. Surface displacement may be masked by manmade modifications, or the fault trace may be displaced to the northeast. In any case, future detailed study of these fans may provide information on main strand displacements and earthquake recurrence interval.

Rattlesnake Mountain fault no. 5 (RMF-5)—RMF-5 forms a moderately strong to strong geomorphic north-south lineament across the southwestern part of the Carnation quadrangle. It is coincident with a strong gravity gradient, thus has likely had some sub-vertical displacement. The fault is associated with Quaternary tectonism and liquefaction of nonglacial deposits in the southernmost part of the map area as well as deformation of Olympia beds in the Fall City quadrangle (Dragovich and others, 2007).

Snoqualmie Valley fault no. 1 (SVF-1)—SVF-1 is inferred to be a major basin-bounding fault in the study area and in the Snoqualmie quadrangle south of the map area. The fault bounds the Snoqualmie and Carnation basins and likely juxtaposes the volcanic rocks of Snoqualmie Falls against older volcanic and metamorphic rocks south of the map area. The SVF-1 is extended to the northwest corner of the map area based upon the geometry of geophysical anomalies. RMF-1 and (or) SVF-1 bounds the Seattle basin as inferred in Cross Sections A and B of Dragovich and others (2010).

Snoqualmie Valley fault no. 2 (SVF-2)—SVF-2 is inferred to be a major basin-bounding fault in the study area. The fault bounds the Carnation basin. Significant tectonic deformation and (or) liquefaction of Pleistocene nonglacial units is observed along this fault in the map area.

Cherry Creek fault zone (CCFZ)—We term a family of subparallel faults in the northeastern part of the quadrangle the Cherry Creek fault zone. Some of these north-northeast trending faults may be seismically active (see May 2, 1996, M_L 5.3 Duvall earthquake in Appendix 8). Local Quaternary deformation of unit Qc_{ol} was observed within this fault zone and may be due to tectonism within the CCFZ. The CCFZ may be a conjugate fault zone to the overall right-lateral and northwest-trending RMFZ. This arrangement is strikingly similar to the relationship between the Tokul Creek fault zone and the RMFZ in the Snoqualmie quadrangle southeast of the present map area and east of the City of Snoqualmie (Dragovich and others, 2009b,c). In both cases the northeast-trending faults may be conjugate faults to the RMFZ-SWIF system where the northeast-trending Tokul Creek fault zone merges with the northwest-trending RMFZ. Tokul Creek fault was originally mapped by Tabor and others (1993)—this regional fault zone juxtaposes basement with or without thin overlying Tertiary volcanic rocks against thicker Tertiary volcanic rocks. Although no distinct lidar lineaments or Quaternary deformation along the Tokul Creek fault were noted by

Dragovich and others (2009b), the occurrence of several earthquake hypocenters near the Tokul Creek fault zone suggests a locally active structure. Earthquake focal mechanism data suggest that this fault zone is currently accommodating left-lateral strike-slip displacement (see Fig. 4 on Plate 2 of Dragovich and others, 2009b).

Carnation faults no. 1 and no.2 (CF)—These faults are inferred on the basis of gravity-magnetic, seismic and earthquake data as discussed in Appendix 8 and above. We elaborate here on the possibility that some geomorphic anomalies within the Snoqualmie River Valley might be related to transpression across the CF or other faults within the RMFZ. Two pertinent observations:

- River valleys floodplains generally increase in width in the downstream direction, but this trend is not observed in the Carnation quadrangle. The Snoqualmie River Valley south of Carnation in the Fall City quadrangle is almost 2 miles wide; the Snoqualmie River Valley north of Carnation quadrangle in the Monroe quadrangle is mostly about 2 miles wide. In contrast, the Snoqualmie River Valley in the Carnation quadrangle between these areas is generally a mile or less wide.
- The Snoqualmie River Valley deviates to the northwest north of the Carnation faults. This arcuate curvature of the river valley north of CF may mimic the inferred trace of these faults near the river valley.

We speculate that the constriction or necking of the valley (as well as the arcuate step of the valley to the northwest) may be related to Quaternary displacements across some of the faults in the area, possibly including south-vergent reverse faulting along the CF. We wonder if this constriction is the result of Quaternary episodic uplift along the upper plate of the CF and trapping of the river within a transpressional segment of the RMFZ-SWIF, perhaps coincident with a restraining bend of the RMFZ-SWIF.

APPENDICES

See Table 1 at the beginning of this document for the filename of electronically attached appendices.

ACKNOWLEDGMENTS

This geologic map was funded in part by the U.S. Geological Survey (USGS) National Cooperative Geologic Mapping Program under award no.G09AC00178. We wish to acknowledge the many and generous contributions of others: Renate Hartog (UW, Pacific Northwest Seismic Network) for help with the earthquake data; the late Lou Lepp (Associated Earth Sciences, Inc.) for unpublished mapping of the Carnation Quadrangle, detailed mapping of selected geotechnical project areas within the quadrangle, and an unpublished radiocarbon age date from Tolt MacDonald Park; Ray Wells (USGS) for financial support; Elizabeth Nesbitt (UW), John Bethel (King County Dept. of Natural Resources) and Tony Burgess (Tony Burgess Consulting) for geologic observations; and Andrei M Sarna-Wojcicki (USGS, emeritus) for pumice microprobe data. We also thank Dennis Armstrong (King County Dept. of Transportation), Russ Steele (Wash. State Dept. of Transportation), and Sue Kahle and Myrtle Jones (USGS, Water Resources Division, Tacoma) for subsurface geologic information, and Albert Gonzales and Mike Leathers (King County Information Technology Division, GIS Products and Services) for the LIDAR data. We also thank our Washington Division of Geology and Earth Resources colleagues for their assistance and patience, including Tim Walsh for helping with the LIDAR maps and data, Fritz Wolff for compiling subsurface information, Robert Berwick for help with file management, and Lee Walking for assistance with references.

REFERENCES CITED

- Advanced National Seismic System, 2010, ANSS Catalog Search, [Accessed on May 16, 2010
<http://www.ncedc.org/anss/catalog-search.html>]
- Aitken, M.J., 1985, Thermoluminescence Dating, London, Academic Press, 359 p.
- Alexander, S. S.; Cakir, R., 2008, Improved hypocenter determinations using the cepstral stacking method (CSM) with

- a dense regional network of stations [abstract]: *Seismological Research Letters*, v. 79, no. 2, p. 295.
- Anderson, M. L.; Blakely, R. J.; Brocher, T. M.; Pratt, T. L.; Wells, R. E.; Haugerud, R.; Bush, M., 2006, Structure of the Seattle uplift from seismic, gravity, magnetic, geologic, and geomorphic data: *Eos (American Geophysics Union Transactions)*, v. 87, no. 52, Supplement, Abstract T41A-1554.
- Associated Earth Sciences, Inc. (AESI), 2001, Subsurface Exploration, Geologic Hazard, and Geotechnical Engineering Report, Trilogy at Redmond Ridge, Project B Vault, West Snoqualmie valley Road NE and Novelty Hill Road, King County, Washington: Prepared for Quadrant Corporation, Project No. KE01105A, March 15, 2001.
- Associated Earth Sciences, Inc. (AESI), 2004, Environmental Impact Statement Technical Report on Geology, Soils and Ground Water, Redmond Ridge East UPD/FCC and Panhandle Preliminary Plat, King County, Washington: Prepared for Quadrant Corporation, Project No. KG02617H, March 31, 2004.
- Associated Earth Sciences, Inc. (AESI), 2002, Final Hydrogeologic and Geotechnical Assessment Report, Pegasus Thoroughbred Training Center, King County, Washington: for Pegasus Thoroughbred Training Center, LLC, Project No. KG01743A, March 1, 2002.
- Associated Earth Sciences, Inc. (AESI), 2007, Summary of SRS-1 No. 1 Infiltration Pond, General Geologic Hazard, and Geotechnical Engineering Recommendations, Recreation Complex, Redmond Ridge East, King County, Washington: Prepared for RR East Partners, Project No. KG070129A, October 31, 2007.
- Bailey, J.C., 1981, Chemical criteria for a refined tectonic discrimination of orogenic andesites: *Chemical Geology*, v. 32, p. 139-154.
- Bhatia, M.R., 1983, Plate tectonics and geochemical composition of sandstones: *Journal of Geology*, v. 91, p. 611-627.
- Bhatia, M.R., and Crook, K.A.W., 1986, Trace element characteristics of graywackes and tectonic setting discrimination of sedimentary basins: *Contributions to Mineralogy and Petrology*, v. 92, p. 181-193.
- Blakely, R. J., 1995, *Potential theory in gravity and magnetic applications*: Cambridge University Press, 441 p.
- Blakely, R. J.; Wells, R. E.; Weaver, C. S., 1999, Puget Sound aeromagnetic maps and data: U.S. Geological Survey Open-File Report 99-514, version 1.0. [<http://geopubs.wr.usgs.gov/open-file/of99-514/>]
- Borchardt, G. A.; Aruscavage, P. J.; Millard, H. T., Jr., 1972, Correlation of the Bishop ash, a Pleistocene marker bed, using instrumental neutron activation analysis: *Journal of Sedimentary Petrology*, v. 42, no. 2, p. 301-306.
- Cakir, Recep; Dragovich, Joe; Walsh, Timothy J.; Hartog, Renate; Alexander, Shelton S.; Anderson, Megan L., 2009, Use of earthquake catalog and waveform data for tectonic mapping in WA [abstract]. IN Northwest Scientific Association, The Pacific Northwest in a changing environment--Northwest Scientific Association 81st annual meeting; Program with abstracts: Northwest Scientific Association, p. 8.
- Capps, Gerald; Simmons, J. D.; Videgar, F. D., 1973, Preliminary report on the geology of southern Snohomish County, Washington: Washington Division of Geology and Earth Resources Open File Report 73-1, 11 p., 2 plates.
- Carlstad, Cynthia A., 1992, Late Pleistocene deglaciation history at Point Partridge, central Whidbey Island, Washington: Western Washington University Master of Science thesis, 1 v.
- Danner, Wilbert Roosevelt, 1957, A stratigraphic reconnaissance in the northwestern Cascade mountains and San Juan Islands of Washington State: University of Washington Doctor of Philosophy thesis, 3 v. [562 p.], 7 plates.
- Dethier, D. P.; Dragovich, J. D.; Sarna-Wojcicki, A. M.; Fleck, R. J., 2008, Pumice in the interglacial Whidbey Formation at Blowers Bluff, central Whidbey Island, WA, USA: *Quaternary International*, v. 178, no. 1, p. 229-237.
- Dethier, D. P.; Sarna-Wojcicki, A. M.; Fleck, R. J., 2005, Interglacial pumice in Whidbey Formation at Blowers Bluff, central Whidbey Island, Washington [abstract]: *Geological Society of America Abstracts with Programs*, v. 37, no. 7, p. 180.
- Dragovich, Joe D.; Petro, Gary T.; Thorsen, Gerald W.; Larson, Sarah L.; Foster, Gregory R.; Norman, David K., 2005, Geologic map of the Oak Harbor, Crescent Harbor, and part of the Smith Island 7.5-minute quadrangles, Island County, Washington: Washington Division of Geology and Earth Resources Geologic Map GM-59, 2 sheets, scale 1:24,000. [accessed Mar. 6, 2008 at http://www.dnr.wa.gov/Publications/ger_gm59_geol_map_oakharbor_crescentharbor_24k.zip]
- Dragovich, J. D., 2007, Sand point count and geochemical data in the Fall City and Carnation 7.5-minute quadrangles, King County, Washington: Washington Division of Geology and Earth Resources Open File Report 2007-3, zip archive containing 3 files, 386 kb. [accessed Sep. 30, 2009 at http://www.dnr.wa.gov/Publications/ger_ofr2007-3_fallcity_supplement.zip]
- Dragovich, J. D.; Anderson, M. L.; Walsh, T. J.; Johnson, B. L.; Adams, T. L., 2007, Geologic map of the Fall City 7.5-minute quadrangle, King County, Washington: Washington Division of Geology and Earth Resources Geologic Map GM-67, 1 sheet, scale 1:24,000.

- Dragovich, Joe D.; Walsh, Timothy J., 2008, Geochemical sample analyses of Tertiary and pre-Tertiary volcanic rocks in and around the North Bend 7.5-minute quadrangle, King County, Washington: Washington Division of Geology and Earth Resources Open File Report 2008-4, 6 p. text with 1 Excel file on DVD. [accessed Feb. 28, 2009 at http://www.dnr.wa.gov/Publications/ger_ofr2008-4_northbend_geochem.zip]
- Dragovich, J. D.; Walsh, T. J.; Anderson, M. L.; Hartog, Renate; DuFrane, S. A.; Vervoot, Jeff; Williams, S. A.; Cakir, Recep; Stanton, K. D.; Wolff, F. E.; Norman, D. K.; Czajkowski, J. L., 2009a, Geologic map of the North Bend 7.5-minute quadrangle, King County, Washington, with a discussion of major faults, folds, and basins in the map area: Washington Division of Geology and Earth Resources Geologic Map GM-73, 1 sheet, scale 1:24,000.
- Dragovich, J. D.; Littke, H. A.; Anderson, M. L.; Hartog, Renate; Wessel, G. R.; DuFrane, S. A.; Walsh, T. J.; MacDonald, J. H., Jr.; Mangano, J. F.; Cakir, Recep, 2009b, Geologic map of the Snoqualmie 7.5-minute quadrangle, King County, Washington: Washington Division of Geology and Earth Resources Geologic Map GM-75, 2 sheets, scale 1:24,000.
- Dragovich, J. D.; Littke, H. A.; MacDonald, J. H., Jr.; DuFrane, S. A.; Anderson, M. L.; Wessel, G. R.; Hartog, Renate, 2009c, Geochemistry, geochronology, and sand point count data for the Snoqualmie 7.5-minute quadrangle, King County, Washington: Washington Division of Geology and Earth Resources Open File Report 2009-4, 35 p. text, 3 Microsoft Excel files; http://www.dnr.wa.gov/Publications/ger_ofr2009-4_snoqualmie_suppl.zip.
- Dragovich, J. D.; Littke, H. A.; Anderson, M. L.; Wessel, G. R.; Koger, C. J.; Saltonstall, J. H.; MacDonald, J. H., Jr.; Mahan, S. A.; DuFrane, S. A., 2010, Geologic map of the Carnation 7.5-minute quadrangle, King County, Washington: Washington Division of Geology and Earth Resources Open File Report 2010-1, 1 sheet, scale 1:24,000, with 21 p. text; http://www.dnr.wa.gov/Publications/ger_ofr2010-1_geol_map_carnation_24k.zip.
- Jones, M. A., 1996, Thickness of unconsolidated deposits in the Puget Sound lowland, Washington and British Columbia: U.S. Geological Survey Water-Resources Investigations Report 94-4133, 1 sheet. [accessed Jan. 14, 2010 at <http://pubs.er.usgs.gov/usgspubs/wri/wri944133>]
- Floyd, P. A.; Shail, R.; Leveridge, B. E.; Franke, W., 1991, Geochemistry and provenance of Rhenohercynian synorogenic sandstones—Implications for tectonic environment discrimination. *In* Morton, A. C.; Todd, S. P.; Haughton, P. D. W., Developments in sedimentary provenance studies: Geological Society [London] Special Publication 57, p. 173-188.
- Forman, S.L., and Pierson, J., 2002, Late Pleistocene luminescence chronology of loess deposition in the Missouri and Mississippi river valleys, United States: *Palaeogeography, Palaeoclimatology, Palaeoecology*, v. 186, no. 1 and 2, p. 25-46.
- Frost, B. R., Barnes, C. G., Collins, W. J., Arculus, R. J., Ellis, D. J., and Frost, C. D., 2001, A geochemical classification for granitic rocks: *Journal of Petrology*, v. 42, p. 2033-2048.
- Galloway, W. E., 1974, Deposition and diagenetic alteration of sandstone in northeast Pacific arc-related basins; implications for greywacke genesis: *Geological Society of America Bulletin*, v. 85, p. 379-390.
- Johnson, D.M., Hooper, P.R., and Conrey, R.M., 1999, XRF analysis of rocks and minerals for major and trace elements on a single low dilution Li-tetraborate bead: *Advances in X-ray Analysis*, v. 41, p. 843-867.
- Koger, C.J. and Saltonstall, J.H., 2009, Maintaining ground water recharge in Master Planned Communities: Case histories from eastern King County, Washington: *Geological Society of America Abstracts with Programs*, Vol. 41, No. 7 (abstract 76-2).
- Koger, C. J., Saltonstall, J. H., Baumgarten, D. J., 2003, Hydrogeology of the eastern Bear Creek plateau, King County, Washington: *Geological Society of America Abstracts with Programs*, Vol. 35, No. 6 (Abstract 201-11).
- Knaack, C., Cornelius, S., and Hooper, P., 1994, trace element analysis of rocks and minerals by ICP/MS: Department of Geology, Washington State University Open-file report, December 1994, 18 p.
- Le Maitre, R.W., ed., 2002, *Igneous rocks. A Classification and Glossary of Terms*, Second edition: Cambridge University Press, Cambridge, U.K., 236p.
- Liberty, Lee M.; Pape, Kristin M., 2006, Seismic characterization of the Seattle and Southern Whidbey Island fault zones in the Snoqualmie River valley, Washington--Final technical report: U.S. Geological Survey Earthquake Hazards Program, External Research Support, Funded Research Final Technical Reports, 17 p. [accessed Mar. 31, 2009 at <http://earthquake.usgs.gov/research/external/reports/06HQGR0111.pdf>]
- Lindquist, John Warren, 1957, Molluscan paleontology of Fiddlers Bluff, Washington: University of Washington undergraduate research thesis, 38 p.
- Lisi, A.; Malone, S. D.; Thomas, G. C., 2000, Precise relative locations for aftershocks of the 1996 Duvall, WA earthquake [abstract]: *Seismological Research Letters*, v. 71, no. 2, p. 237.
- Littke, H. A.; Dragovich, J. D.; Anderson, Megan; Hartog, Renate; Wessel, G. R.; Dufrane, S. A.; Walsh, T. J.;

- MacDonald, J. H., Jr.; Cakir, Recep, 2009, Geologic map of the Snoqualmie 7.5-minute quadrangle, King County, Washington--Active faulting, basin inversion and Miocene volcanic extrusion of the Snoqualmie batholith along the Rattlesnake Mountain fault zone [abstract]: Geological Society of America Abstracts with Programs, v. 41, no. 7, p. 457.
- Mahan, S.A., Miller, D.M., Menges, C.M., and Yount, J.C., 2007, Late Quaternary stratigraphy and luminescence geochronology of the northeastern Mojave Desert, Quaternary International, vol. 166, pp. 61-78.
- Mahoney, B.J., Prindiville, S., Troost, K.G., and Booth, D.B., 2003, Geochemical characteristics of glaciogenic sediments, Puget Lowland, Washington: Geological Society of America Abstracts with Programs, v.35, n.6, p.79.
- Mahoney, J. B., 2007, Quaternary sediments geochemical analytical data—Redmond Ridge East UPD/FCC and Panhandle preliminary plat [prepared for Associated Earth Sciences, Inc.]: J. Brian Mahoney unpublished report, 51
- Marcus, Kim L., 1981, The rocks of Bulson Creek--Eocene-Oligocene sedimentation and tectonics in the Lake McMurray area, Washington: Western Washington University Master of Science thesis, 84 p., 1 plate.
- McDonough, W.F., and Sun, S.S., 1995, The composition of the Earth: Chemical Geology, v. 120, p. 223-253.
- McLennan, S. M., 1989, Rare earth elements in sedimentary rocks—Influence of provenance and sedimentary processes: Reviews in Mineralogy and Geochemistry, v. 21, no. 1, p. 169-200.
- McLennan, S. M., 2001, Relationships between the trace element composition of sedimentary rocks and upper continental crust: Geochemistry, Geophysics, Geosystems - G 3, 2, p. 2000GC000109.
- McLennan, S. M., Taylor, S. R., McCulloch, Malcolm T., and Maynard, J. B., 1990, Geochemical and Nd-Sr isotopic composition of deep-sea turbidites; crustal evolution and plate tectonic associations: *Geochimica et Cosmochimica Acta*, v. 54, p. 2015-2050.
- McLennan, S. M.; Hemming, S.; McDaniel, D. K.; Hanson, G. N., 1993, Geochemical approaches to sedimentation, provenance, and tectonics. *In* Johnson, M. J.; Basu, A., eds., Processes controlling the composition of clastic sediments: Geological Society of America Special Paper 284, p. 21-40.
- Minard, J. P.; Booth, D. B., 1988, Geologic map of the Redmond quadrangle, King County, Washington: U.S. Geological Survey Miscellaneous Field Studies Map MF-2016, 1 sheet, scale 1:24,000.
- Murray, A.S., Marten, R., Johnston, A., and Martin, P., 1987, Analysis for naturally occurring radionuclides at environmental concentrations by gamma spectrometry: *Journal of Radioanalytical and Nuclear Chemistry*, Article 115, p. 263-288.
- Pearce, J. A., 1982, Trace element characteristics of lavas from destructive plate boundaries: in Thorpe, R. S., ed., *Andesites; orogenic andesites and related rocks*, p. 525-548.
- Pearce, J.A., 1983, Role of the subcontinental lithosphere in magma genesis at active continental margins, in Haworth, C.J., and Norry, M.J., eds., *Continental basalts and mantle xenoliths*: Nantwich, Great Britain, Shiva Publishing, p. 230-249.
- Polenz, Michael; Slaughter, Stephen L.; Thorsen, Gerald W., 2005, Geologic map of the Coupeville and part of the Port Townsend North 7.5-minute quadrangles, Island County, Washington: Washington Division of Geology and Earth Resources Geologic Map GM-58, 1 sheet, scale 1:24,000. [accessed Mar. 6, 2008 at http://www.dnr.wa.gov/Publications/ger_gm58_geol_map_coupeville_24k.pdf]
- Prescott, J. R. and Hutton, J.T., 1994, Cosmic ray contributions to dose rates for luminescence and ESR dating: large depths and long-term time variations: *Radiation Measurements*, v. 23, p. 497-500.
- Prothero, D.R., Nesbitt, E.A. 2009, Paleomagnetism and tectonic rotation of the Restoration Point member of the Blakeley Formation (type Blakeley stage), Bainbridge Island, Washington, and the Pacific Coast Oligocene-Miocene boundary: *New Mexico Museum of Natural History and Science Bulletin* 44, p. 315-323.
- Rau, W. W., and S. Y. Johnson (1999). Well stratigraphy and correlations, western Washington and northwest Oregon, U.S. Geol Surv Map Invest. I-2621, (3 sheets).
- Richardson, C.A., McDonald, E.V. and Busacca, A.J., 1997, Luminescence dating of loess from the northwest United States: *Quaternary Science Reviews*, v. 16, no. 3-5, p. 403-415.
- Roser, B. P., and Korsch, R. J., 1986, Determination of tectonic setting of sandstone-mudstone suites using SiO₂ content and K₂O/Na₂O ratios: *Journal of Geology*, v. 94, p. 635-650.
- Roser, B. P., and Korsch, R. J., 1988, Provenance signatures of sandstone-mudstone suites determined using discriminant function analysis of major-element data: *Chemical Geology*, v. 67, p. 119-139.
- Saltonstall, J. H., Koger, C. J., Sweet, S., and Thompson, S. S., 2003, Olympia age paleotopographic influences on Vashon glaciofluvial sedimentation beneath the eastern Bear Creek plateau, King County, Washington: Geological

- Society of America Abstracts with Programs, Vol. 35, No. 6 (Abstract 42-4).
- Singhvi, A.K., Sharma, Y.P. and Agrawal, D.P., 1982, Thermo-Luminescence Dating of Sand Dunes in Rajasthan, India: *Nature*, v. 295 (5847), p. 313-315.
- Simonetti, Antonio; Heaman, L. M.; Hartlaub, R. P.; Creaser, R. A.; MacHattie, T. G.; Bohm, Christian, 2005, U-Pb zircon dating by laser ablation-MC-ICP-MS using a new multiple ion counting Faraday array: *Journal of Analytical Atomic Spectrometry*, v. 20, no. 8, p. 677-686.
- Sherrod, B. L.; Blakely, R. J.; Weaver, C. S.; Kelsey, H. M.; Barnett, Elizabeth; Liberty, Lee; Meagher, K. L.; Pape, Kristin, 2008, Finding concealed active faults—Extending the Southern Whidbey Island fault across the Puget Lowland, Washington: *Journal of Geophysical Research*, v. 113, B05313, doi:10.1029/2007JB005060, 2008.
- Snyder, S.L., and Duval, J.S., 2003, Design and construction of a Gamma-ray Spectrometer system for determining natural radioactive concentrations in geological samples at the U.S. Geological Survey in Reston, Virginia, U.S. Geological Survey Open-File Report 03-29 (on-line only) (<http://pubs.usgs.gov/of/2003/of03-029/>).
- Tabor, R. W.; Frizzell, V. A., Jr.; Booth, D. B.; Waitt, R. B.; Whetten, J. T.; Zartman, R. E., 1993, Geologic map of the Skykomish River 30- by 60-minute quadrangle, Washington: U.S. Geological Survey Miscellaneous Investigations Series Map I-1963, 1 sheet, scale 1:100,000, with 42 p. text. [<http://geopubs.wr.usgs.gov/i-map/i1963/>]
- Thomas, G. C.; Crosson, R. S.; Cohee, B. P.; Qamar, A. I.; Lombard, P., 1996, The May 2, 1996, Duvall, Washington earthquake and aftershock sequence [abstract]: *Eos (American Geophysical Union Transactions)*, v. 77, no. 46, Supplement, p. F523.
- Wyss, M., Wiemer, S. and Zuniga, R., 2001, ZMAP a tool for analyses of seismicity patterns - typical applications and uses: A cook book. [<http://www.earthquake.ethz.ch/software/zmap/cookbook.pdf>].
- Yount, J. C.; Gower, H. D., 1991, Bedrock Geologic Map of the Seattle 30 by 60 Quadrangle, Washington: U.S. Geological Survey Open-File Report 91-147, 37 p., 4 plates.